

Exact Constraint of Density Functional Approximations at the Semiclassical Limit

Yunzhi Li¹ and Chen Li^{1,*}

¹*Beijing National Laboratory for Molecular Sciences,
College of Chemistry and Molecular Engineering, Peking University, Beijing 100871, China
(Dated: January 7, 2025)*

ABSTRACT: We introduce the semiclassical limit to electronic systems by taking the limit $\hbar \rightarrow 0$ in the solution of Schrödinger equations. We show that this limit is closely related to one type of strong correlation that is particularly challenging from conventional multi-configurational perspective but can be readily described through semiclassical analysis. Furthermore, by studying the performance of density functional approximations (DFAs) in the semiclassical limit, we find that mainstream DFAs have erroneous divergent energy behaviors as $\hbar \rightarrow 0$, violating the exact constraint of finite energy. Importantly, by making connection of the significantly underestimated DFA energies of many strongly correlated transition-metal diatomic molecules to their rather small estimated \hbar_{eff} , we demonstrate the usefulness of our semiclassical analysis and its promise for inspiring better DFAs.

I. INTRODUCTION

Density functional theory (DFT) with the existing approximations has been extremely successful in describing weakly correlated systems, ranging from atoms, molecules to metallic solids. Through introducing an auxiliary non-interacting system,¹ Kohn-Sham DFT is endowed with the physical picture of independent electrons moving in a mean field, which is essentially valid for most of the main-group compounds of chemical interests. In such a way, the complicated many-body wave function is effectively reduced to N occupied orbitals. This crucial simplification makes life so much easier in terms of both theory and computation that chemists cannot live without the concept of orbitals since the early days of quantum mechanics until the present day. However, there is one class of challenging systems where the single-electron orbital picture breaks down, known as strongly correlated systems. Typical examples of strongly correlated systems include stretched molecules and transition-metal compounds,^{2–4} where the correlation cannot be captured by perturbative treatment to any single Slater determinant, and one cannot find a dominant determinant in the configuration interaction (CI) expansion of the many-body wave function.^{5–8} Strong correlation can also occur in solid materials, such as Mott insulators,^{9–14} where the strong electron–electron interaction leads to the breakdown of the band structure theory.¹⁵

It is crucial to note that the above-mentioned challenges should not be regarded as failures of density functional theory, which by the Hohenberg-Kohn formulation¹⁶ is formally exact. Instead, problem arises in the exchange-correlation (xc) functional in the Kohn-Sham decomposition of the total energy, whose exact form cannot be obtained explicitly and in practical calculations has to be treated by density functional approximations (DFAs). It is the qualitatively incorrect behaviors of these DFAs, characterized by the violation of some important conditions or constraints,

that are responsible for their failures in strongly correlated systems. Among other exact constraints, one important constraint relevant for strong correlation is the fractional spin (FS) condition.^{3,17} In particular, the strong correlation problem of a stretched molecule is understood from the perspective that local spin densities of an isolated fragment integrate to a fractional number, a problematic scenario where DFAs tend to overestimate the energy. Along this line of thinking, functionals have been constructed to restore the local FS condition, which can then properly describe molecular dissociation.¹⁸ However, for unstretched molecules such as well-bonded metal oxides, how one should perform the FS analysis remains a major challenge.

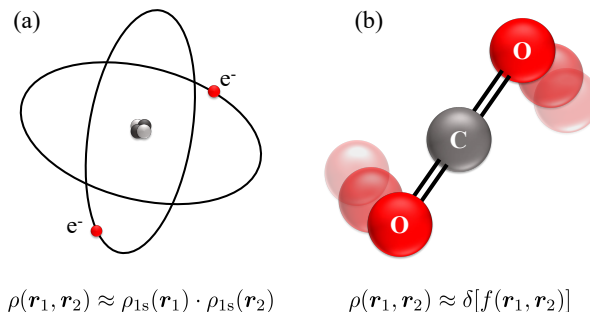


Figure 1. Schematic illustration of the weakly and strongly correlated picture: (a) two electrons independently orbit around the helium nucleus, representative of a weakly correlated picture; (b) two oxygen atoms rotate around the carbon atom in collective motion in a CO_2 molecule, representative of a strongly correlated picture.

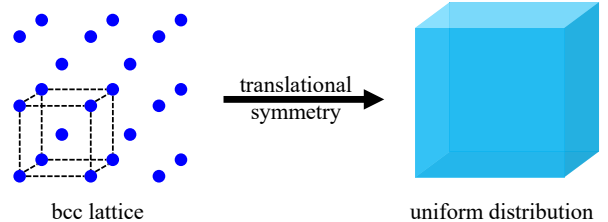
To gain more insight into the problem of strong correlation, let us take one step back and review the physical nature of weak and strong correlation through an example of a two-particle system. In a weakly correlated picture such as the electrons in a helium

atom in its ground state, the electronic motions are almost independent from each other, pictorially shown as in Fig. 1(a). It follows from the probability theory that the joint probability of finding one electron at \mathbf{r}_1 and the other at \mathbf{r}_2 is given by the following product, $\rho(\mathbf{r}_1, \mathbf{r}_2) \approx \rho_{1s}(\mathbf{r}_1)\rho_{1s}(\mathbf{r}_2)$, where $\rho_{1s}(\mathbf{r})$ is the probability of finding an electron in the 1s orbital. In the case of strong correlation, in contrast, the joint probability $\rho(\mathbf{r}_1, \mathbf{r}_2)$ becomes a δ function. This is because the motions of the two electrons are strongly entangled; if one knows the position of one particle, then one immediately knows the position of the other. Interpreted physically, having motions of collective rather than of individual nature, is what distinguishes strong correlation from weak correlation. Such a picture is reminiscent of atoms in a molecule within the semiclassical treatment. We can remind ourselves of the linear CO_2 molecule as shown in Fig. 1(b), where the two oxygen atoms are strongly entangled as they always appear equidistantly on the opposite sides of the carbon atom.

The fact that the strong correlation limit and the semiclassical limit has a lot in common is not a coincidence. Here let us remind ourselves that in the most general sense semiclassical limit is defined by taking a small \hbar -related dimensionless quantity to zero;¹⁹ this quantity can be \hbar itself or a combination of \hbar and other parameters such as the nuclear mass. In CO_2 , because the nuclear kinetic energy T_n is much smaller than the potential energy V (due to the much heavier nuclear mass compared to the electronic mass), as a good approximation by Born and Oppenheimer,²⁰ we can neglect T_n and treat the nuclei as clamped at their classical positions. This forms a major contrast with the electrons, for which the kinetic energy T is for most cases on the same order of magnitude as V . However, there are exceptions. A famous example is the uniform electron gas (UEG) in the low density limit, where V dominates over T such that electrons behave like semiclassical particles that crystalize to form a lattice, known as the Wigner crystal.^{21–23} Fig. 2 (a) is an illustration of the Wigner crystal for a body-centered cubic (bcc) lattice. In the design of the simplest local density approximation (LDA) to the correlation energy by Vosko, Wilk and Nusair (VWN5),^{24,25} the correct limiting behaviors for low as well as high density UEG have already been built in the functional. In this sense, it comes as no surprise that LDA can properly describe metallic solids even though some metals are presumably strongly correlated- such systems are not so distinct from the UEG.

For atoms and molecules, however, the idealization of UEG or Wigner crystal barely occurs because the electron density is usually far from uniform distribution. Nevertheless, we can still borrow the idea we learned from Wigner crystal and define a semiclassical limit, which we refer to as the “Wigner atom/molecule” highlighting the non-uniform density distribution and finite boundary condition. Here we achieve this by taking the limit $\hbar \rightarrow 0$ to the solution of the Schrödinger equation, which is

(a) Wigner crystal



(b) “Wigner atom/molecule”

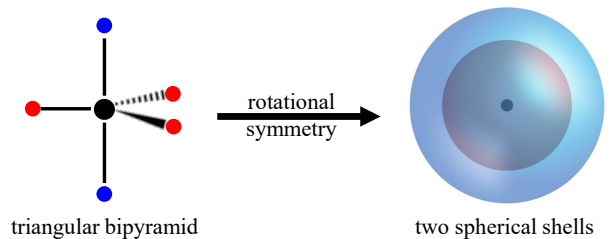


Figure 2. Schematic illustration comparing (a) Wigner crystal and (b) a 5-electron “Wigner atom”. In (b), electrons crystalize at two types of classical positions surrounding the nucleus (in black), as shown by the red and blue dots, respectively. After considering the rotational symmetry, they form two spherical shells.

essentially to make T negligibly small compared to V . A schematic illustration is given in Fig. 2 (b), where five electrons condense into classical positions [electron density becomes a sum of delta functions, see Eq. (5)] and form a triangular bipyramid structure as $\hbar \rightarrow 0$, in order to reach the minimum potential energy. When rotational symmetry is considered, the electron density shall evenly distribute on two spherical shells, with the radii corresponding to the two electron-nuclear distances of the triangular bipyramid.

Through this definition, we can study the exact constraint of DFAs at the semiclassical limit. We will show that mainstream DFAs all suffer from qualitatively wrong asymptotic behavior in approaching this limit. Moreover, by estimating the effective \hbar for real molecules, we establish a semi-quantitative relation between the error of LDA [and also generalized gradient approximations (GGAs)] and \hbar_{eff} . In particular, we find that there is a strong correlation between the large error of DFAs and small \hbar_{eff} , particularly for transition metal compounds. Before we go into details of our theory, it is worth mentioning the strictly correlated electron (SCE) theory developed by Seidl and Gori-Giorgi et al,^{26–31} which also discusses intensively the exact functional in the strong correlation limit for molecular systems. Differing from the present work that focuses on the exact conditions violated by DFAs for v -representable densities, the SCE theory focuses on the exact functional form defined for all N -

representable densities through the constrained search formula. The resulting form of the SCE functional involves complicated co-motion functions, which without further approximations poses challenges for practical calculations beyond a few electrons.²⁷ In this paper, we take a different route. By identifying the missing exact semiclassical constraints important for strongly correlated molecules, we hope to guide functional approximations that improve mainstream DFAs for these systems by recovering the correct limit.

II. THEORY

A. Effective \hbar for real molecules

Let us start by considering the following many-electron Hamiltonian under an external one-body potential V_{ext} ,

$$\left[-\frac{1}{2} \sum_i \nabla_i^2 + \sum_i V_{\text{ext}}(\mathbf{r}_i) + \sum_{i<j} \frac{1}{|\mathbf{r}_i - \mathbf{r}_j|} \right] \Psi = E\Psi, \quad (1)$$

At first glance, it seems that there is no playground to introduce an adjustable \hbar or take the semiclassical limit, because \hbar is a physical constant and set to 1 in atomic unit for real molecules. In the following, we show that an effective \hbar can be introduced in two ways.

The first way is through scaling the coordinates by $\mathbf{r}'_i \equiv \hbar^2 \mathbf{r}_i$ such that we can introduce $\hbar \neq 1$ as an adjustable parameter lesser than 1. The resulting SE reads

$$\left[-\frac{\hbar^2}{2} \sum_i \nabla_i'^2 + \sum_i \frac{1}{\hbar^2} V_{\text{ext}}\left(\frac{1}{\hbar^2} \mathbf{r}'_i\right) + \sum_{i<j} \frac{1}{|\mathbf{r}'_i - \mathbf{r}'_j|} \right] \Psi = E'\Psi. \quad (2)$$

Here $E' \equiv E/\hbar^2$. Eq. (2) corresponds to an auxiliary system with one-body potential $V'_{\text{ext}}(\mathbf{r}) = \frac{1}{\hbar^2} V_{\text{ext}}(\frac{1}{\hbar^2} \mathbf{r})$. Compared with the original system, the external potential is squeezed and deepened; see Fig. 3 (a) for an illustration. Through introducing this auxiliary potential V'_{ext} , one can bridge a strongly correlated system of normal $\hbar = 1$ with a semiclassical system with $\hbar \rightarrow 0$; they are equivalent in the sense that their wave functions (and also electron densities) only differ by a scaling of the coordinates. As a real-world example, a dissociated normal H_2 molecule with internuclear distance $R = 74 \text{ \AA}$ is equivalent to a compact H_2 with $R' = 0.74 \text{ \AA}$ and scaled $\hbar = 0.1$, as shown in Fig. 3 (b). The scaled system with normal bondlength but deepened potential is as strongly correlated as the dissociated H_2 with normal $\hbar = 1$. Therefore, looking into the scaled system from the semiclassical perspective shall give us good insight into the increasingly correlated physics as the molecule approaches its dissociation limit. Moreover, when evaluating DFAs for the scaled density, we shall invoke the inverse mapping from the scaled

system to the normal system with $\hbar = 1$ and plug in the unscaled density, which will be discussed in subsequent subsections.

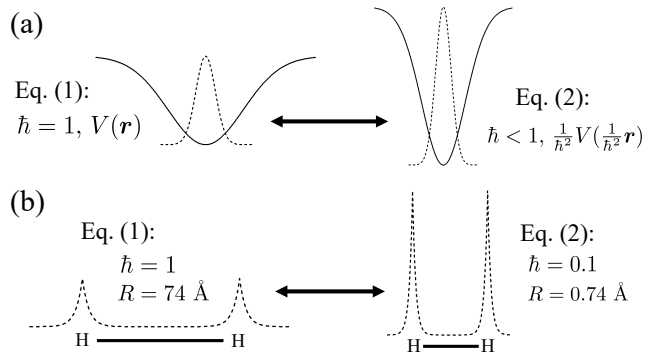


Figure 3. Visualization of the connection between the two systems defined by Eq. (1) and Eq. (2). Here (a) is a schematic illustration of a general problem, where the solid lines represent the external potentials and dashed lines represent the ground state densities; (b) gives a concrete example of a dissociated H_2 molecule (only densities are shown).

For correlations that occur in a compact molecule such as a metal oxide, however, the above scaling argument cannot lead to useful semiclassical picture. For such systems, a useful way of introducing effective \hbar is to map the system to an exactly solvable model problem with adjustable \hbar . In particular, by tuning the \hbar of the model system until one finds the largest resemblance with the real molecular system in the natural occupation distributions, one can define this particular \hbar to be the effective \hbar of the molecule of interest. In this work, we choose as our model system the harmonium problem (also known as the Hooke's helium), whose Hamiltonian is given by

$$\hat{H} = -\frac{\hbar^2}{2} (\nabla_1^2 + \nabla_2^2) + \frac{1}{2} \omega^2 (r_1^2 + r_2^2) + \frac{1}{r_{12}}. \quad (3)$$

In our recent work, we have obtained the following compact analytic formula for its ground state:³²

$$\Psi(\mathbf{r}_1, \mathbf{r}_2) = C \left(1 + \frac{r_{12}}{c}\right)^\gamma e^{-\frac{\omega(r_1^2 + r_2^2)}{2\hbar}} G\left(\frac{r_{12}}{r_{12} + c}\right), \quad (4)$$

Here C is the normalization constant, $\gamma = \frac{E}{\hbar\omega} - 3$ with E being the energy, and $c > 0$ is a parameter that one can choose in a reasonable range; G is a series function whose expansion coefficients (dependent on \hbar, ω and c) can be analytically obtained. Eq. (4) is valid for any parameter \hbar and ω and can be evaluated to arbitrary accuracy with a reasonable cost. For some particular parameters, G reduces to a polynomial, as was found in the literature.³³ Here of particular interest is the distribution of natural occupation numbers and its evolution with \hbar , as it is an indicator of how strongly electrons are

correlated. With the analytic expression of Eq. (4), this can be computed very easily; the result is shown in Fig. 4. When \hbar is large, essentially only the 1s orbital is doubly occupied, which is a weakly correlated regime where the wave function is well described by a single Slater determinant. When \hbar is small and approaches 0, Fig. 4 shows that all natural orbitals are fractionally occupied. Moreover, each orbital is occupied by a tiny little bit whereas these tiny numbers sum up to an integer 2. If we translate this picture to the language of CI expansion, it means that the wave function is composed of infinitely many Slater determinants while none of them dominates. This is qualitatively different from the conventional static correlation picture where the wave function is always dominated by a finite number of determinants, such as in a stretched molecule. As a consequence, the semiclassical limit of harmonium (in fact for other systems as well) is an extremely hard situation for conventional multi-configuration based methods such as MRCI or CASSCF; as shown in Ref.³² one needs an astronomical number of determinants to obtain a reasonable accuracy. With our subsequent semiclassical analysis of Eq. (6), however, the correct semiclassical limit can be easily recovered. This suggests that with the very different physical pictures as in Fig. 1(a) and (b), it might be beneficial to use distinct starting point to develop theory.

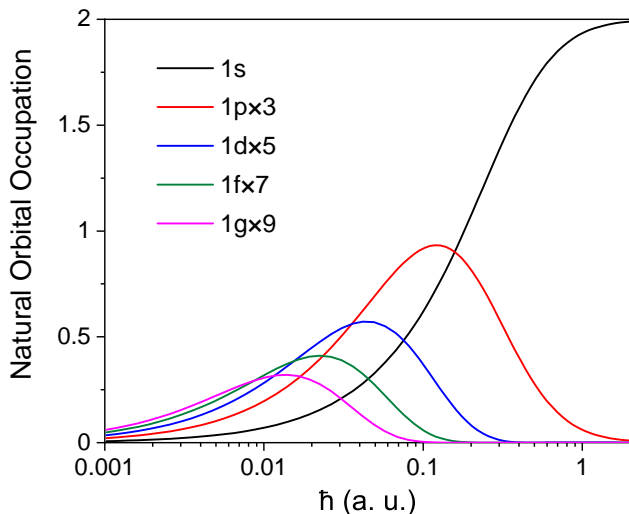


Figure 4. Evolution of the occupation number distribution over selected natural orbitals (multiplied by their respective degeneracy) with \hbar for the ground state of harmonium ($\omega = 0.373$).

The criteria for defining the largest resemblance of natural occupation distribution is not unique. Although such a distribution is system dependent, we highlight the following general structures: aligned in decreasing order, the natural occupations of a general system is given by $1, 1, 1, \dots, n_H, n_L, \dots, 0, 0, \dots$, where the largest numbers are close to 1 and the smallest numbers

close to 0 and all these numbers sum up to the total number of electrons N . In this work, we choose $\tau = \frac{n_L}{n_H}$ as the mapping variable that bridges a real-world system to the model harmonium problem, where n_H and n_L are the occupation number of the N th and $(N + 1)$ th spin-dependent natural orbitals, respectively. The corresponding natural orbitals can be viewed as analogues of the highest occupied molecular orbital (HOMO) and lowest unoccupied molecular orbital (LUMO). Moreover, we choose $\omega = 0.373$ for the benchmarking harmonium such that when $\hbar = 1$ the mapping variable τ agrees with that of a normal H_2 at bondlength $R = 0.74\text{\AA}$. The resulting benchmarking curve of \hbar_{eff} as a function of τ is shown in Fig. 5, where we highlight the small τ region relevant for chemistry. For a real-world molecule, by performing a CASSCF calculation we can compute the approximate many-body wave function and obtain its natural occupation numbers and τ . By looking up the value of this particular τ in Fig. 5, we can read out its \hbar_{eff} . Some representative atom and diatomic molecules have been marked along the benchmarking curve. For example, by our definition H_2 molecule with $\hbar_{\text{eff}} = 1$ is a typical weakly-correlated system; He atom with $\hbar_{\text{eff}} = 1.45$ has even weaker correlation. ZnO with $\hbar_{\text{eff}} \approx 0.5$ lies at the boundary line between weakly and strongly correlated systems. With even smaller \hbar_{eff} of about 0.2, C_2 and Cr_2 are typical strongly correlated systems. These results are in line with our chemical intuition.

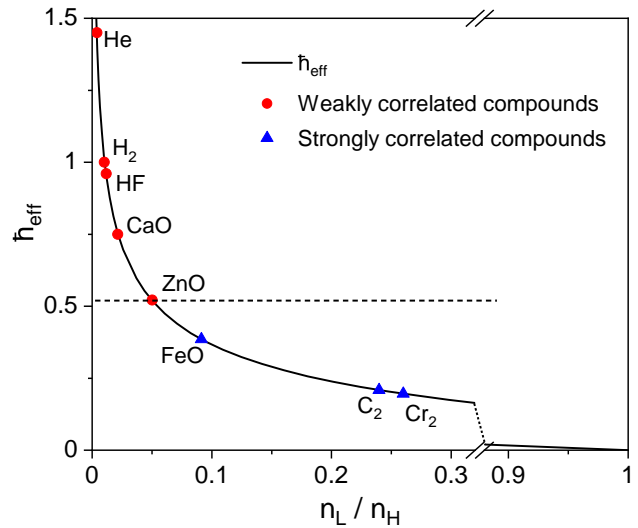


Figure 5. Benchmarking curve showing the mapping relation between \hbar_{eff} and $\tau = \frac{n_L}{n_H}$, which is obtained from the model harmonium calculation with $\omega = 0.373$. Marked along the curve are some representative atoms and diatomic molecules.

To establish a semi-quantitative relation between the error of DFAs with the magnitude of correlation of small and medium-sized molecules, in Fig. 5 we present a scatter plot of the bond dissociation energy (BDE)

error of the Perdew-Burke-Ernzerhof (PBE) functional³⁴ against \hbar_{eff} for 172 data points from the well-known datasets documented in the literature.^{7,35–38} The scatter plot for LDA shows similar trend, see the supplemental information (SI) for details.³⁹ As shown in Fig. 6, \hbar_{eff} of these molecules range from 0.2 to 1.1, while the energy errors range from a few kcal/mol up to 42 kcal/mol. We highlight that the distribution of these data points are not completely random, instead, most of them scatter in a lower triangular region underneath the green reference line. This suggests that the general trend is that the error drops as \hbar_{eff} increases. Moreover, we have drawn two dashed boxes in black and blue, respectively, which contain the majority of the data points. Specifically, most of the weakly correlated main group compounds (black dots) lie in the black box where \hbar_{eff} is closer to 1 rather than 0, and the PBE errors are relatively small. These account for the majority (60%) of the molecules tested, where PBE works well. By contrast, molecules with a large error (over 16.5 kcal/mol) account for 28% of the data points, and a large proportion of these molecules (mainly transition-metal compound marked as blue dots), falling into the blue box, are strongly correlated in the sense of having \hbar_{eff} closer to 0 rather than 1, and their energies are all underestimated. As a side remark, some molecules (red dots) in our examined dataset composed of main group elements have been classified as having multireference character. Here in our plot, they have smaller \hbar_{eff} in the general trend than those that are classified as in the non-multireference subset (black dots). However, the errors of these red dots are not significantly larger than the black dots. We believe this is because some strong correlation effect has already been built in the PBE correlation functional through satisfying some limiting conditions, such as the low density limit of HEG, which allows it to partially capture the correlation for non-uniform densities. This could also be used to explain the blue dots that fall outside the black and blue box. Despite these outliers, we emphasize that molecules in the blue box are our targets, for which we attempt to understand their errors through semiclassical analysis of the functional forms of mainstream DFAs.

B. Exact behavior of energy and density at the semiclassical limit

Let us group all the potential energy in Eq. (1) as $V_{\text{tot}} = \sum_{i=1}^N V_{\text{ext}}(\mathbf{r}_i) + \sum_{i<j} \frac{1}{r_{ij}}$. Assuming for a moment that $V_{\text{ext}}(\mathbf{r})$ is bounded from below such that the many-body potential V_{tot} has a minimum, which is the case for harmonium. In the limit $\hbar \rightarrow 0$, solving the quantum mechanical ground state energy of such a system reduces to the minimization of V_{tot} , and the ground state electron

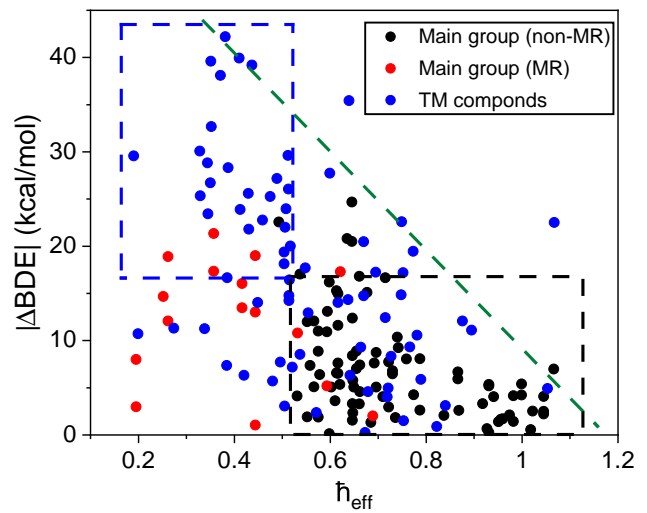


Figure 6. Scatter plot illustrating the correlated relation between \hbar_{eff} and the error of PBE functional on the prediction of bond dissociation energies (BDEs). Black and red dots: nonmultireference and multireference subsets, respectively, of the BDE99 dataset^{7,35} composed of main group elements. Blue dots: diatomic molecules containing third-row transition-metals (TMs), including TM hydrides,³⁶ oxides,³⁷ nitrides and dimers.³⁸ The dashed line and boxes serve as guides of the eye, highlighting the general trend; see the text for details.

density becomes a sum of δ -functions,

$$\rho(\mathbf{r}) = \sum_i \delta(\mathbf{r} - \mathbf{r}_i^0), \quad (5)$$

where $(\mathbf{r}_1^0, \mathbf{r}_2^0, \dots, \mathbf{r}_N^0)$ is the minimizer of V_{tot} . In the presence of degeneracy induced by rotation symmetry such as in harmonium, the summation in Eq. (5) shall be replaced by integration. The physical picture is shown in Fig. 2(b), where electrons condense at their classical positions.

When \hbar is not zero but sufficiently small, the above picture shall be amended to allow electronic vibrations within a narrow range around their classical positions, analogous to the harmonic oscillator approximation (HOA) of nuclear vibrational problems. In particular, by expanding V_{tot} in Taylor series around the classical positions up to the second order and then diagonalizing the Hessian matrix, one can obtain the normal modes and the corresponding frequencies ω . It can be shown that the energy obtained within HOA, call it $E_{\text{gs}}^{\text{HOA}}$, captures the leading order of \hbar correction to the total energy,³⁹

$$E_{\text{gs}}^{\text{exact}} = E_{\text{gs}}^{\text{HOA}} + \mathcal{O}(\hbar^2). \quad (6)$$

The electron density is also broadened from a sum of δ -functions to Gaussian-type distributions around the classical positions.

C. DFA behaviors in semiclassical atomic models

The harmonium problem provides us an ideal playground for testing the performance of DFAs in the semiclassical limit. Using the exact wave function as given by Eq. (4), we can compute the exact density. One can show that the density has spherical symmetry; by integrating out the Euler angles, it can be expressed as the following integration over r' :

$$\rho(\mathbf{r}) = \frac{Be^{-2\alpha r^2}}{r} \int_0^\infty dr' \times r'(1 + \frac{r'}{c})^{2\gamma} e^{-\alpha r'^2} \sinh(2\alpha r r') G^2\left(\frac{r'}{r' + c}\right). \quad (7)$$

Here $\alpha = \frac{\omega}{\hbar}$ and $B = 8C^2 \sqrt{\frac{2\alpha}{\pi}}$. Shown in Fig. 7 is the evolution of the exact density with \hbar . For weakly correlated case such as when $\hbar = 1$, the density peaks at the origin. As \hbar decreases, the enhanced electron correlation induces a shoulder in the density profile, which gradually develops into a Gaussian-type distribution for diminishing \hbar . This is in line with our HOA analysis. In particular, one can deduce the following Gaussian behavior for small \hbar ,

$$\rho^{\text{HOA}}(\mathbf{r}) \propto \exp\left[-\frac{\omega_0}{\hbar}(r - r_0)^2\right], \quad (8)$$

where $r_0 = (2\omega)^{-2/3}$ is the semiclassical electron-nuclear distance and $\omega_0 = (3 - \sqrt{3})\omega$ is a radial harmonic frequency extracted from the normal mode. Our HOA analysis has been confirmed numerically; see the increasingly better agreement between the dashed and solid lines for diminishing \hbar as shown in Fig. 7: ρ^{HOA} is an extremely good approximation to the exact density for small \hbar ; and as $\hbar \rightarrow 0$, Eq. (8) approaches a δ -function.

With the exact density, we plug it into DFAs and study the functional error in the semiclassical limit. As we have suggested in subsection A, one needs to extend the xc functionals, which were designed for $\hbar = 1$, to arbitrary \hbar . This is achieved through the coordinate scaling as illustrated in Fig. 3. For a system with $\hbar \neq 1$ and density ρ_\hbar , we can map it back to a normal system with $\hbar = 1$ and density ρ_1 , with the scaling relation $\rho_1(\mathbf{r}) = \hbar^6 \rho_\hbar(\hbar^2 \mathbf{r})$. The energy E_1 can then be evaluated by plugging ρ_1 into the functional form of DFAs. Finally from the energy scaling argument we can obtain $E_\hbar = \frac{E_1}{\hbar^2}$. After simplifying the resulting energy expression and singling out the xc functional, we find that it satisfies the following scaling relation:³⁹

$$E_{xc,\hbar}[\rho_\hbar(\mathbf{r})] = \frac{1}{\hbar^2} E_{xc,1}[\rho_1(\mathbf{r})]. \quad (9)$$

The total energy of DFAs as function of \hbar are shown in Fig. 8. Compared with the exact curve, DFAs perform

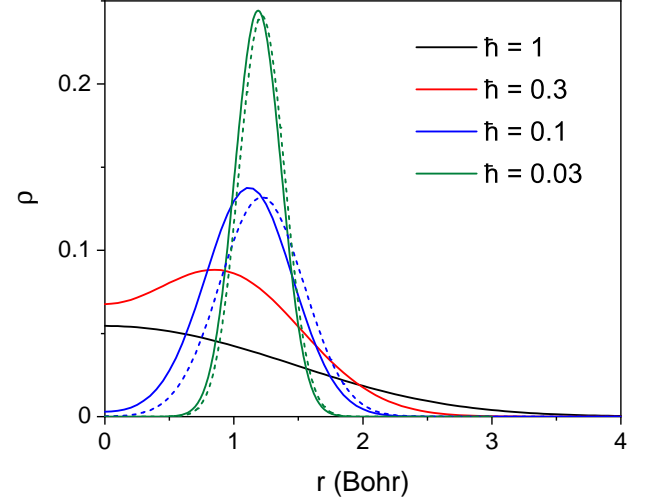


Figure 7. Evolution of the exact ground state density (solid lines) of harmonium with decreasing \hbar . The HOA densities (dashed lines) calculated by Eq. (8) are also shown for some small \hbar for comparison.

very well for the most part (all lines almost overlap each other), particularly when \hbar is not small. This is because for weakly correlated systems with 2 electrons, the xc energy is a small term compared to the other three Kohn-Sham energy components that are defined as known and explicit functionals of the density, namely the Kohn-Sham kinetic energy, external energy and the Hartree energy. Then essentially any mainstream DFA can be a decent approximation to the total energy. For small \hbar , however, divergent behavior starts to emerge. In particular, LDA, GGAs exemplified by PBE and the Lee-Yang-Parr (BLYP) functional, and the hybrid B3LYP functional^{40,41} all diverge to minus infinity in the limit $\hbar \rightarrow 0$. By contrast, the Hartree-Fock (HF) functional converges to a finite value because it is derivable from a variational wave function theory and shall always overestimate the exact total energy, which is finite in the semiclassical limit and given by the minimum of V_{tot} .

Using HOA, we can derive the asymptotic behavior of LDA exchange as $\mathcal{O}(\hbar^{-\frac{1}{6}})$.³⁹ This divergent behavior can be attributed to the local exchange energy that is proportional to $\rho^{4/3}$: as ρ approaches δ -function, ρ^α integrates to infinity for any $\alpha > 1$. Similar analysis can also be performed for the VWN5 correlation functional, although analytic derivation becomes more difficult. By numerical fitting, we find it also diverges as $\mathcal{O}(\hbar^{-\frac{1}{6}})$.³⁹ Therefore, for LDA we have

$$E_{\text{atom}}^{\text{LDA}} = C_1 \hbar^{-1/6} + \mathcal{O}(1), \quad (10)$$

which violates the following exact constraint:

$$E_{\text{atom}}^{\text{exact}} = C_0 + \mathcal{O}(\hbar). \quad (11)$$

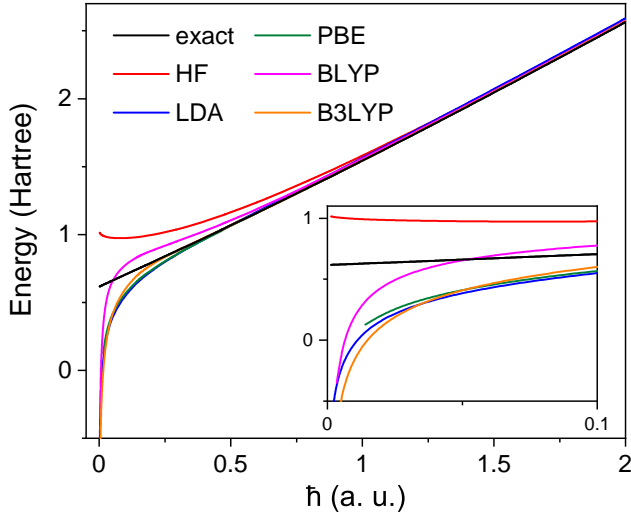


Figure 8. Ground state energy of harmonium (with $\omega = 0.373$) as function of \hbar calculated with some mainstream DFAs, in comparison with the exact one. The inset shows an enlarged plot for the small- \hbar region. PBE results for very small \hbar are not shown due to the limited numerical precision of Libxc.⁴²

For real-world atoms with Coulombic nuclear attraction potentials, our semiclassical analysis cannot be directly applied to Eq. (1) because V_{ext} and also V_{tot} are not bounded from below. Nevertheless, let us remind ourselves that the most essential part of correlation occurs among valence electrons; core electrons such as those occupying 1s orbitals are rather inert and only weakly correlated with other electrons. The idea of separating the core from the valence electrons has lead to various approximation schemes, such as the pseudopotential method,⁴³ the complete active space self-consistent field (CASSCF) method,^{44–46} and the recently proposed electronic exact factorization in the Fock space.⁴⁷ Due to the Pauli exclusion from the core electrons, valence electrons are unlikely to appear in the vicinity of the nuclei; the resulting effective potential (or pseudopotential) replaces the bare Coulomb divergence by a short-range repulsion, giving rise to a potential minimum.

Here we use the bulk-derived local pseudopotential (BLPS)⁴⁸ developed by Carter et al as V_{ext} and perform semiclassical analysis for the valence electrons of magnesium (2 electrons) and arsenic atom (5 electrons), respectively. Although the exact density can no longer be obtained easily for arbitrary \hbar , we can use the density from HOA analysis to generate meaningful results when \hbar is small. In particular, when $\hbar \rightarrow 0$, the density is distributed on a single shell for model Mg atom, similar to the harmonium problem, but spread on two spherical shells for model As atom [see Fig. 2 (b)]. With a finite \hbar , the density broadens into Gaussian-type functions

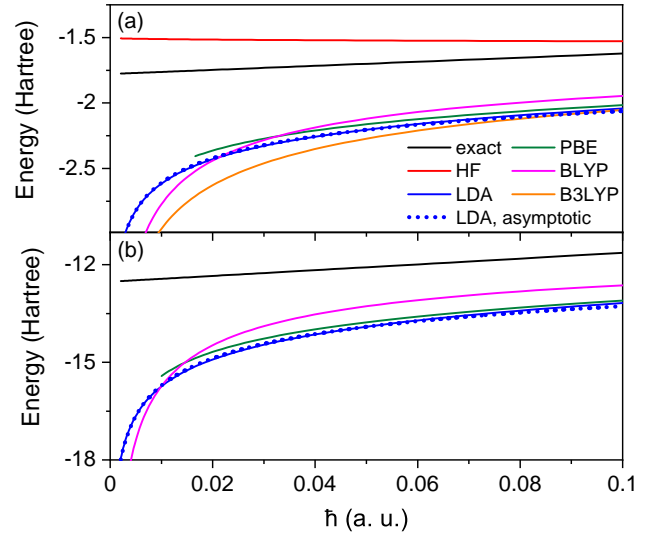


Figure 9. Total energy as function of \hbar in the small- \hbar region for (a) model Mg atom and (b) model As atom under pseudopotential. DFAs are compared with the exact curve under HOA. The asymptotic expansion of Eq. (10) with fitted expansion coefficients up to $\mathcal{O}(1)$ is shown in blue dotted line for comparison. In (b), the Hartree–Fock and B3LYP results are not shown; see our remarks in the text.

analogous to Fig. 7, and well approximated by HOA. By plugging ρ^{HOA} into the functional form of DFAs, we can show that this approximation introduces small error that is of higher-order to $\mathcal{O}(1)$; see Fig. 9. This is only slightly larger than the HOA error in the exact curve, which has additional $\mathcal{O}(\hbar)$ term included through harmonic analysis according to Eq. (11). Comparing with the exact finite behavior in the semiclassical limit, again we can come to the conclusion that DFAs all diverge as $\mathcal{O}(\hbar^{-\frac{1}{6}})$, violating the exact constraint similar to the harmonium problem. As a side remark, we note that in the evaluation of DFAs, the Kohn–Sham kinetic energy is neglected because it is $\mathcal{O}(\hbar)$. Besides, the Hartree–Fock exchange energy is an explicit functional of the Kohn–Sham orbitals rather than the density. From the density alone for more than 2 electrons, one needs to invoke the optimized effective potential (OEP)^{49,50} techniques to obtain HF or B3LYP results, which are not the focus of the present paper and thus not shown. For spin unpolarized 2-electron systems, the doubly occupied Kohn–Sham orbital is the square root of the density so that HF exchange can be computed straightforwardly. Details can be found in the SI.³⁹

D. DFA behaviors in semiclassical molecular models

Our semiclassical analysis can also be performed for molecules. As an example, let us consider a single-bond stretching problem of a diatomic molecule. Again,

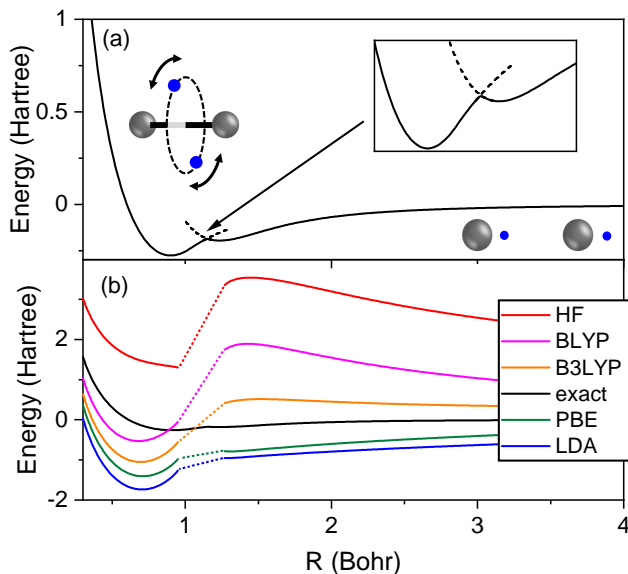


Figure 10. (a) Dissociation energy curve along with the semiclassical pictures showing bonding and bond-breaking regimes of a model 2-electron diatomic molecule as $\hbar \rightarrow 0$. The adiabatic energy curve is shown in solid line whereas the diabatic curves are displayed in dashed lines near the crossing point. (b) Ground state energy of the same model with $\hbar = 0.01$. Here DFAs under HOA are compared with the exact curve that is accurate up to $\mathcal{O}(\hbar)$. The DFA results in the dotted region are not shown; see remarks in the text.

we focus on the two bonding electrons, which are modeled through our self-designed effective electron-nuclear potential.³⁹ In contrast to the atomic model, here the change of $V_{\text{tot}}(\mathbf{r}_1, \mathbf{r}_2, R)$ with the internuclear distance R leads to interesting physical picture of bond-forming and bond-breaking in the semiclassical limit. In particular, for small R , minimization of V_{tot} with respect to the electronic variables gives a bonding picture where the two electrons localize on the opposite sides of a ring that bisects the two nuclei, reminiscent of the shared electron pair in our routinely used Lewis structure. For large R , bonding picture is energetically unfavorable; instead, the minimum energy is achieved by localizing the electrons in the vicinity of the nuclei, giving a typical bond-breaking picture. The resulting semiclassical energy as a function of R along with the schematic pictures are shown in Fig. 10 (a). As one can expect, there is a critical R at the transition of the two pictures, corresponding to a crossing point of the diabatic curves and a cusp in the adiabatic curve. For finite \hbar , this cusp is rounded out; see for example the black curve in Fig. 10 (b). We highlight that such a shift of picture is rather insensitive to the choice of effective electron-nuclear potential, although it does affect the fine details of transition. As an additional remark, the emergence of the critical point in the semiclassical limit reminds us of the Coulson—Fischer point⁵¹ well-known in the

dissociation of H_2 for normal \hbar , where the unrestricted Hartree-Fock calculation switches between two types of solutions. We suspect that there is an internal connection and that the “phase transition” type of behavior might be widespread in the dissociation of molecules and may trigger new understanding of chemical bonds. For example, the peculiar behavior of the dissociation energy curve of chromium dimer⁵² might be due to smoothed-out “phase transitions” of multiple bond-breaking stages. We leave this for future investigations.

Table 1. Asymptotic leading order (with its sign specified if possible) of LDA energy components in the limit $\hbar \rightarrow 0$ for model atoms and diatomic molecules.

	Atom	Diatomic molecule
V_{ext}	$\mathcal{O}(1)$	$\mathcal{O}(1)$
T_s	$+\mathcal{O}(\hbar)$	$+\mathcal{O}(\hbar)$
J	$+\mathcal{O}(1)$	$+\mathcal{O}(\ln \hbar)$
E_{xc}^{LDA}	$-\mathcal{O}(\hbar^{-1/3})$	$-\mathcal{O}(\hbar^{-1/3})$
$E_{\text{tot}}^{\text{LDA}}$	$-\mathcal{O}(\hbar^{-1/3})$	$-\mathcal{O}(\hbar^{-1/3})$
$E_{\text{tot}}^{\text{exact}}$	$\mathcal{O}(1)$	$\mathcal{O}(1)$

Inspired by the exact semiclassical solution, we next perform semiclassical analysis for DFAs with $\hbar = 0.01$; see Fig. 10 (b). Depending on the semiclassical picture of bonding or bond-breaking, the HOA density can be qualitatively different. Thus we discuss these two regimes separately. For small R , DFAs typically underestimate the total energy. In analogy to the atomic model, one can rationalize this deviation by deriving the asymptotic expansion of the LDA energy with \hbar for bonded diatomic molecules as³⁹

$$E_{\text{mol}}^{\text{LDA}} = C_1 \hbar^{-1/3} + \mathcal{O}(|\ln \hbar|). \quad (12)$$

Here the leading terms are due to the xc and Hartree term, respectively. Further details of the asymptotic leading order of each component of the LDA functional is tabulated in Table 1, where we have also compared between atomic and diatomic molecular models. As in the case of atoms, here LDA violates the exact constraint of finite total energy in approaching the semiclassical limit, and other DFAs suffer from similar failures. As R is stretched towards the diabatic crossing point, the anharmonic terms of V_{tot} become increasingly important such that our HOA density becomes a bad approximation to the exact density. In such cases, we have not found simple alternative ways of approximating the exact density to plug into the functional forms of DFAs. Therefore, DFA results in this part of the dissociation curve are not shown, instead, we replace them with dotted lines. Beyond this region, HOA revives as a valid approximation, but gives distinct density as suggested in Fig. 10 (a). For such density, DFAs exhibit diversified behaviors, which is not our focus. In the dissociation limit, they all overestimate the total energy (not shown),

in line with the fractional-spin analysis.³

Comparing Eq. (10) and Eq. (12), atoms and molecules have distinct semiclassical divergent behaviors for LDA. In particular, the leading term of $-\mathcal{O}(\hbar^{-\frac{1}{3}})$ for diatomic molecules diverges faster than the atomic behavior of $-\mathcal{O}(\hbar^{-\frac{1}{6}})$. This is because the molecular density is more concentrated- two electrons spread their density as delta function on a ring rather than on two spherical shells around the two nuclei, which accelerates the divergence of the xc integral. As a consequence, one can immediately deduce that LDA always overbinds diatomic molecules when \hbar is sufficiently small. For \hbar that is not small, unsurprisingly it is well-known that LDA tends to overbind real-world molecules with $\hbar = 1$.^{7,35,36,53} Previously this has been understood from the perspective of delocalization error.³ Here we provide a novel perspective which ascribes the overbinding to the violation of an exact constraint at the semiclassical limit. A further fact that supports our argument is the systematic and severe overbinding of LDA among strongly correlated transition metal diatomic molecules, for which an LDA+ U correction is often needed.^{4,14,54,55} The empirical U correction is positive in most cases, and the more strongly correlated systems demand a larger U correction. This can be well explained using our semiclassical argument: the stronger the correlation, the smaller the \hbar_{eff} , which pushes the system closer to the semiclassical limit where the violation of the exact constraint has the largest consequence. Our conclusions derived from LDA also apply to GGAs since they have rather similar behaviors.

III. CONCLUSION

In this work, we introduce semiclassical limit to electronic systems, where the reduced Planck constant \hbar is treated as an adjustable parameter and tends to 0. Compared with the conventional understanding of strong correlation through multi-configurational picture, our semiclassical perspective along with the concept of \hbar_{eff} provides a novel insightful picture, which could offer a better starting point for method development. Besides the conceptual conciseness, our semiclassical limit is particularly pertinent to describing the type of strong correlation that involves combinatorial number of “democratic” determinants while no one takes the lead. Such a scenario could arise from the partially-filled degenerate d orbitals of transition metals and near-degenerate orbitals of nearby atoms in their compounds, and is an extremely hard situation from the multi-configurational perspective. It is perhaps even harder for perturbation theory if one starts with a mean field. The conventional approaches, which are suitable for treating one or a handful of determinants, are simply too far from capturing the essence of this type of strong correlation physics. For such problems, instead of using orbitals describing individual motion, we propose to switch to the

collective motion of strongly correlated electrons through HOA in the semiclassical treatment, which is a many-body description by design.

In contrast to another “semiclassical” regime discussed by Burke et al.,^{56–61} which scales the electron number to infinity upon taking $\hbar \rightarrow 0$, our semiclassical limit has totally opposite physics of strong correlation rather than weak correlation. In similar spirit to the Wigner crystal for periodic solids, our semiclassical limit could be regarded as its extension to finite systems, where electrons condense at classical positions defined by the minimum of total potential energy. Instead of explaining why DFAs work well in the weakly correlated limit as exemplified by a neutral atom with large nuclear charge,^{57,62–64} here with our semiclassical regime we aim to find the important missing constraint of DFAs responsible for their qualitative failures in strongly correlated molecules. In particular, DFAs significantly underestimate total energy in the semiclassical limit. For example, the exchange-correlation energy of LDA erroneously diverges to minus infinity as $\mathcal{O}(\hbar^{-1/6})$ for model atoms and $\mathcal{O}(\hbar^{-1/3})$ for model diatomic molecules. This can explain the overbinding of LDA and GGAs for strongly correlated transition metal diatomic molecules since we have estimated that the effective \hbar for the valence electrons of these systems can be quite small.

The concept of \hbar_{eff} proposed in this work comes from the physical consideration that core electrons are well-separated energetically from other electrons and contribute little to the valence correlation that is relevant to chemistry. Therefore, the effective \hbar for valence electrons does not have to agree with the reduced Planck constant for all-electrons. Here we aim to introduce \hbar_{eff} as a quantitative indicator to characterize the extent of correlation of a particular system. This allows us to compare correlations among different systems rather than vaguely referring all of them to as strongly correlated systems. In this sense, \hbar_{eff} can be a useful concept for describing a system, just like other physically sound but empirical chemical concepts such as bond order or hardness of Lewis acids, which can be appealing to chemists although not uniquely defined. In this work, we define \hbar_{eff} by mapping the natural occupation numbers of real-world molecules to model harmonium problem via the relation $\frac{n_L}{n_H} \rightarrow \hbar$. This particular choice gives reasonable \hbar_{eff} for the molecules tested. Yet, chances are that one might find other mappings that yield better agreement with our chemical intuition.

As a final remark, we expect the exact semiclassical constraint for E_{xc} proposed in this work can give us important hint for improving the energy prediction of transition metal compounds. For these challenging systems, the known exact conditions for strong correlation, such as the well-established flat plane condition for fractional charges and spins,⁶⁵ have not found an easy path to be applicable. So far the successful application of these conditions is mainly to

alleviate molecular dissociation problems where DFAs can be improved by restoring the underlying condition for local subsystems using the fractional-spin local orbital scaling correction (FSLOSC) functional.¹⁸ However, the picture of local fractional spins, derived from isolated subsystems perfect valid in the dissociation limit, becomes ambiguous in unstretched molecules where subsystems come together and form chemical bonds. In such cases, switching to our semiclassical perspective may inspire new functional development. Along this line of thinking, a critical task is to extract the information of \hbar_{eff} from DFAs. If \hbar_{eff} is not small, then little correction is needed. Otherwise, a positive correction should be imposed to the xc energy to counterbalance its underestimated behavior. We leave this for future investigations.

Supporting Information See the supplemental information at xxx for some details.

Acknowledgment

The authors appreciate funding support from the National Key Research and Development Program of China (2023YFA1507000) and the National Natural Science Foundation of China (8200906190).

Conflict of Interest

We have no conflicts of interest to disclose.

Data Availability

The data that support the findings of this study are available from the corresponding authors upon reasonable request.

References

-
- * chenlichem@pku.edu.cn
- (1) Kohn, W.; Sham, L. J. Self-Consistent Equations Including Exchange and Correlation Effects. *Phys. Rev.* **1965**, *140*, A1133–A1138.
 - (2) Chan, B.; Gill, P. M. W.; Kimura, M. Assessment of DFT Methods for Transition Metals with the TMC151 Compilation of Data Sets and Comparison with Accuracies for Main-Group Chemistry. *J. Chem. Theory Comput.* **2019**, *15*, 3610–3622.
 - (3) Cohen, A. J.; Mori-Sánchez, P.; Yang, W. Insights into Current Limitations of Density Functional Theory. *Science* **2008**, *321*, 792–794.
 - (4) Kulik, H. J.; Marzari, N. Systematic study of first-row transition-metal diatomic molecules: A self-consistent DFT+U approach. *J. Chem. Phys.* **2010**, *133*.
 - (5) Cohen, A. J.; Mori-Sánchez, P.; Yang, W. Challenges for Density Functional Theory. *Chem. Rev.* **2012**, *112*, 289–320.
 - (6) Becke, A. D. Perspective: Fifty years of density-functional theory in chemical physics. *J. Chem. Phys.* **2014**, *140*, 18A301.
 - (7) Mardirossian, N.; Head-Gordon, M. Thirty years of density functional theory in computational chemistry: an overview and extensive assessment of 200 density functionals. *Mol. Phys.* **2017**, *115*, 2315–2372.
 - (8) Bulik, I. W.; Henderson, T. M.; Scuseria, G. E. Can Single-Reference Coupled Cluster Theory Describe Static Correlation? *J. Chem. Theory Comput.* **2015**, *11*, 3171–3179.
 - (9) Mott, N. F.; Peierls, R. Discussion of the paper by de Boer and Verwey. *Proc. Phys. Soc.* **1937**, *49*, 72.
 - (10) Mott, N. F. Metal-Insulator Transition. *Rev. Mod. Phys.* **1968**, *40*, 677–683.
 - (11) Imada, M.; Fujimori, A.; Tokura, Y. Metal-insulator transitions. *Rev. Mod. Phys.* **1998**, *70*, 1039–1263.
 - (12) Boer, J. H. d.; Verwey, E. J. W. Semi-conductors with partially and with completely filled 3d-lattice bands. *Proc. Phys. Soc.* **1937**, *49*, 59.
 - (13) Zaanen, J.; Sawatzky, G. A.; Allen, J. W. Band gaps and electronic structure of transition-metal compounds. *Phys. Rev. Lett.* **1985**, *55*, 418–421.
 - (14) Kulik, H. J. Perspective: Treating electron overdelocalization with the DFT+U method. *J. Chem. Phys.* **2015**, *142*.
 - (15) Kotliar, G.; Vollhardt, D. Strongly Correlated Materials: Insights From Dynamical Mean-Field Theory. *Phys. Today* **2004**, *57*, 53–59.
 - (16) Hohenberg, P.; Kohn, W. Inhomogeneous Electron Gas. *Phys. Rev.* **1964**, *136*, B864–B871.
 - (17) Cohen, A. J.; Mori-Sánchez, P.; Yang, W. Fractional spins and static correlation error in density functional theory. *J. Chem. Phys.* **2008**, *129*.
 - (18) Su, N. Q.; Li, C.; Yang, W. Describing strong correlation with fractional-spin correction in density functional theory. *Proc. Natl. Acad. Sci. U.S.A.* **2018**, *115*, 9678–9683.
 - (19) Landsman, N. P. In *Philosophy of Physics*; Butterfield, J., Earman, J., Eds.; North-Holland: Amsterdam, 2007; pp 417–553.
 - (20) Born, M.; Oppenheimer, R. Zur Quantentheorie der Molekeln. *Ann. Phys.* **1927**, *389*, 457–484.
 - (21) Wigner, E. On the Interaction of Electrons in Metals. *Phys. Rev.* **1934**, *46*, 1002–1011.
 - (22) Wigner, E. Effects of the electron interaction on the energy levels of electrons in metals. *Trans. Faraday Society* **1938**, *34*, 678–685.
 - (23) Carr, W. J. Energy, Specific Heat, and Magnetic Properties of the Low-Density Electron Gas. *Phys. Rev.* **1961**, *122*, 1437–1446.
 - (24) Ceperley, D. M.; Alder, B. J. Ground State of the Electron Gas by a Stochastic Method. *Phys. Rev. Lett.* **1980**, *45*, 566–569.
 - (25) Vosko, S. H.; Wilk, L.; Nusair, M. Accurate spin-dependent electron liquid correlation energies for local spin density calculations: a critical analysis. *Can. J. Phys.* **1980**, *58*, 1200–1211.
 - (26) Vuckovic, S.; Wagner, L. O.; Mirtschink, A.; Gori-Giorgi, P. Hydrogen Molecule Dissociation Curve with Functionals Based on the Strictly Correlated Regime. *J. Chem. Theory Comput.* **2015**, *11*, 3153–3162.
 - (27) Vuckovic, S.; Gerolin, A.; Daas, K. J.; Bahmann, H.; Friesecke, G.; Gori-Giorgi, P. Density functionals based on the mathematical structure of the strong-interaction limit of DFT. *WIREs Computational Molecular Science*

- 2023**, *13*, e1634.
- (28) Seidl, M.; Gori-Giorgi, P.; Savin, A. Strictly correlated electrons in density-functional theory: A general formulation with applications to spherical densities. *Phys. Rev. A* **2007**, *75*, 042511.
 - (29) Seidl, M. Strong-interaction limit of density-functional theory. *Phys. Rev. A* **1999**, *60*, 4387–4395.
 - (30) Gori-Giorgi, P.; Vignale, G.; Seidl, M. Electronic Zero-Point Oscillations in the Strong-Interaction Limit of Density Functional Theory. *J. Chem. Theory Comput.* **2009**, *5*, 743–753.
 - (31) Buttazzo, G.; De Pascale, L.; Gori-Giorgi, P. Optimal-transport formulation of electronic density-functional theory. *Phys. Rev. A* **2012**, *85*, 062502.
 - (32) Yao, W.; Yin, Z.; Li, C. Formally Exact and Practically Useful Analytic Solution of Harmonium. *ACS Omega* **2024**, *9*, 46138–46147.
 - (33) Taut, M. Two electrons in an external oscillator potential: Particular analytic solutions of a Coulomb correlation problem. *Phys. Rev. A* **1993**, *48*, 3561–3566.
 - (34) Perdew, J. P.; Burke, K.; Ernzerhof, M. Generalized Gradient Approximation Made Simple. *Phys. Rev. Lett.* **1996**, *77*, 3865–3868.
 - (35) Karton, A.; Daon, S.; Martin, J. M. L. W4-11: A high-confidence benchmark dataset for computational thermochemistry derived from first-principles W4 data. *Chem. Phys. Lett.* **2011**, *510*, 165–178.
 - (36) Moltved, K. A.; Kepp, K. P. Chemical Bond Energies of 3d Transition Metals Studied by Density Functional Theory. *J. Chem. Theory Comput.* **2018**, *14*, 3479–3492.
 - (37) Moltved, K. A.; Kepp, K. P. The Chemical Bond between Transition Metals and Oxygen: Electronegativity, d-Orbital Effects, and Oxophilicity as Descriptors of Metal–Oxygen Interactions. *J. Phys. Chem. C* **2019**, *123*, 18432–18444.
 - (38) Furche, F.; Perdew, J. P. The performance of semilocal and hybrid density functionals in 3d transition-metal chemistry. *J. Chem. Phys.* **2006**, *124*.
 - (39) See the Supplemental Material at xxx for further details.
 - (40) Becke, A. D. Density-functional thermochemistry. III. The role of exact exchange. *J. Chem. Phys.* **1993**, *98*, 5648–5652.
 - (41) Lee, C.; Yang, W.; Parr, R. G. Development of the Colle-Salvetti correlation-energy formula into a functional of the electron density. *Phys. Rev. B* **1988**, *37*, 785–789.
 - (42) Lehtola, S.; Steigemann, C.; Oliveira, M. J. T.; Marques, M. A. L. Recent developments in libxc — A comprehensive library of functionals for density functional theory. *SoftwareX* **2018**, *7*, 1–5.
 - (43) Schwerdtfeger, P. The Pseudopotential Approximation in Electronic Structure Theory. *ChemPhysChem* **2011**, *12*, 3143–3155.
 - (44) Werner, H.; Meyer, W. A quadratically convergent multiconfiguration–self-consistent field method with simultaneous optimization of orbitals and CI coefficients. *J. Chem. Phys.* **1980**, *73*, 2342–2356.
 - (45) Werner, H.; Meyer, W. A quadratically convergent MCSCF method for the simultaneous optimization of several states. *J. Chem. Phys.* **1981**, *74*, 5794–5801.
 - (46) Werner, H.; Knowles, P. J. A second order multiconfiguration SCF procedure with optimum convergence. *J. Chem. Phys.* **1985**, *82*, 5053–5063.
 - (47) Requist, R.; Gross, E. K. U. Fock-Space Embedding Theory: Application to Strongly Correlated Topological Phases. *Phys. Rev. Lett.* **2021**, *127*, 116401.
 - (48) Huang, C.; Carter, E. A. Transferable local pseudopotentials for magnesium, aluminum and silicon. *Phys. Chem. Chem. Phys.* **2008**, *10*, 7109–7120.
 - (49) Talman, J. D.; Shadwick, W. F. Optimized effective atomic central potential. *Phys. Rev. A* **1976**, *14*, 36–40.
 - (50) Sharp, R. T.; Horton, G. K. A Variational Approach to the Unipotential Many-Electron Problem. *Phys. Rev.* **1953**, *90*, 317–317.
 - (51) Coulson, C. A.; Fischer, I. Notes on the molecular orbital treatment of the hydrogen molecule. *Phil. Mag.* **1949**, *40*, 386–393.
 - (52) Larsson, H. R.; Zhai, H.; Umrigar, C. J.; Chan, G. K.-L. The Chromium Dimer: Closing a Chapter of Quantum Chemistry. *Journal of the American Chemical Society* **2022**, *144*, 15932–15937.
 - (53) Kohn, W.; Becke, A. D.; Parr, R. G. Density Functional Theory of Electronic Structure. *J. Phys. Chem.* **1996**, *100*, 12974–12980.
 - (54) Anisimov, V. I.; Zaanen, J.; Andersen, O. K. Band theory and Mott insulators: Hubbard U instead of Stoner I. *Phys. Rev. B* **1991**, *44*, 943–954.
 - (55) Liechtenstein, A. I.; Anisimov, V. I.; Zaanen, J. Density-functional theory and strong interactions: Orbital ordering in Mott-Hubbard insulators. *Phys. Rev. B* **1995**, *52*, R5467–R5470.
 - (56) Elliott, P.; Lee, D.; Cangi, A.; Burke, K. Semiclassical Origins of Density Functionals. *Phys. Rev. Lett.* **2008**, *100*, 256406.
 - (57) Okun, P.; Burke, K. *Density Functionals for Many-Particle Systems*; 2023; pp 179–249.
 - (58) Burke, K. Leading correction to the local density approximation of the kinetic energy in one dimension. *J. Chem. Phys.* **2020**, *152*.
 - (59) Burke, K. Deriving approximate functionals with asymptotics. *Faraday Discuss.* **2020**, *224*, 98–125.
 - (60) Cangi, A.; Lee, D.; Elliott, P.; Burke, K. Leading corrections to local approximations. *Phys. Rev. B* **2010**, *81*, 235128.
 - (61) Ribeiro, R. F.; Burke, K. Deriving uniform semiclassical approximations for one-dimensional fermionic systems. *J. Chem. Phys.* **2018**, *148*.
 - (62) Fournais, S.; Lewin, M.; Solovej, J. P. The semi-classical limit of large fermionic systems. *J. P. Calc. Var.* **2018**, *57*, 105.
 - (63) Schwinger, J. Thomas-Fermi model: The leading correction. *Phys. Rev. A* **1980**, *22*, 1827–1832.
 - (64) Constantin, L. A.; Fabiano, E.; Laricchia, S.; Della Sala, F. Semiclassical Neutral Atom as a Reference System in Density Functional Theory. *Phys. Rev. Lett.* **2011**, *106*, 186406.
 - (65) Mori-Sánchez, P.; Cohen, A. J.; Yang, W. Discontinuous Nature of the Exchange-Correlation Functional in Strongly Correlated Systems. *Phys. Rev. Lett.* **2009**, *102*, 066403.

Supporting Information of

Exact Constraint of Density Functional Approximations at the Semiclassical Limit

Yunzhi Li and Chen Li

*Beijing National Laboratory for Molecular Sciences, College of Chemistry and Molecular
Engineering, Peking University, Beijing 100871, China*

(Dated: January 7, 2025)

Contents

I. Some details of the semiclassical limit for many-electron systems	1
II. Supplementary results of \hbar_{eff} calculations	4
III. Some details of DFA calculations in the semiclassical limit	9
IV. Some details of the asymptotic leading term of LDA	11
V. Supplementary figure showing our effective potential for diatomic molecular model	14
References	15

I. SOME DETAILS OF THE SEMICLASSICAL LIMIT FOR MANY-ELECTRON SYSTEMS

Here we show that in the semiclassical regime (\hbar is small), the ground state energy can be well described by harmonic oscillator approximation (HOA), with the error on the order of \hbar^2 . We begin with the following Schrödinger equation,

$$\hat{H}\Psi \equiv \left[-\frac{\hbar^2}{2} \sum_{i=1}^N \nabla_i^2 + \sum_{i=1}^N V_{\text{ext}}(\mathbf{r}_i) + \sum_{i<j} \frac{1}{r_{ij}} \right] \Psi = E\Psi. \quad (\text{S1})$$

Here $V_{\text{tot}} \equiv \sum_{i=1}^N V_{\text{ext}}(\mathbf{r}_i) + \sum_{i<j} \frac{1}{r_{ij}}$ denotes the total potential energy. For the ease of discussion, let us first consider the spinless problem. Later, we will come back to the problem with spin and show that the spin degrees of freedom only affect higher-order terms in the semiclassical expansion.

Assuming that minimization of V_{tot} is achieved at $\mathbf{u} = (\mathbf{r}_1^0, \mathbf{r}_2^0, \dots, \mathbf{r}_N^0)$, yielding minimum potential energy V_0 . Here $\mathbf{r}_i^0 \neq \mathbf{r}_j^0$ for any $i \neq j$, otherwise V_0 cannot be finite. Because V_{tot} has permutation symmetry, its minimizer is not unique. In particular, any permutation of \mathbf{u} (with $N!$ possibilities), denoted as $\mathbf{u}_p = (\mathbf{r}_{p_1}^0, \mathbf{r}_{p_2}^0, \dots, \mathbf{r}_{p_N}^0)$, is also a minimum. We then perform Taylor expansion at one of these minima, similar to the many-body vibrational problem. Here V_{tot} is analogous to the many-body potential energy surface that depends on $3N$ electronic cartesian coordinates. By harmonic analysis, i.e., diagonalizing the $3N \times 3N$ Hessian, one can obtain the harmonic oscillator frequencies ω_k and the normal coordinates q_k ; each q_k is a collective coordinate involving all $3N$ cartesian coordinates. The Schrödinger equation then becomes

$$\left[-\frac{\hbar^2}{2} \sum_{k=1}^{3N} \frac{\partial^2}{\partial q_k^2} + \frac{1}{2} \sum_{k=1}^{3N} \omega_k^2 q_k^2 + V_{\text{anh}}(q_1, q_2, \dots, q_{3N}) \right] \Psi = (E - V_0) \Psi, \quad (\text{S2})$$

where V_{anh} is the anharmonic contribution of V_{tot} . In Eq. (S2), the kinetic energy operator is a small term in the semiclassical limit, which in principle can be treated perturbatively. However, directly performing perturbation theory with \hbar leads to problematic series. To avoid this difficulty, we transform Eq. (S2) into a simpler problem through scaling the collective coordinates by $t_k = \frac{q_k}{\sqrt{\hbar}}$, which gives

$$\left[-\frac{1}{2} \sum_{k=1}^{3N} \frac{\partial^2}{\partial s_k^2} + \frac{1}{2} \sum_{k=1}^{3N} \omega_k^2 t_k^2 + \sqrt{\hbar} \tilde{V}_{\text{anh},3} + \hbar \tilde{V}_{\text{anh},4} + \dots \right] \Psi = E' \Psi. \quad (\text{S3})$$

Here $E' = (E - V_0)/\hbar$; and we have expanded V_{anh} in multi-dimensional Taylor series of t_k 's, with the leading order terms being cubic terms, collected as $\sqrt{\hbar} \tilde{V}_{\text{anh},3}$, and the next leading terms are quartic terms, collected as $\hbar \tilde{V}_{\text{anh},4}$, and so on. Neglecting higher orders of $\sqrt{\hbar}$, we then perform perturbation expansion in $\sqrt{\hbar}$ for the ground state energy and wave function. The zeroth-order wave function (also known as the HOA wave function) is a product of $3N$ harmonic oscillator functions, given by

$$\Psi_0 = \prod_{k=1}^{3N} \left(\frac{\omega_k}{\pi \hbar} \right)^{\frac{1}{4}} \exp \left(-\frac{1}{2} \omega_k t_k^2 \right), \quad (\text{S4})$$

with the zeroth-order energy

$$E'_0 = \frac{1}{2} \sum_k \omega_k. \quad (\text{S5})$$

The 1st-order perturbation correction, given by $\langle \Psi_0 | \sqrt{\hbar} \tilde{V}_{\text{anh},3} | \Psi_0 \rangle$, shall vanish. This is because Ψ_0 has even parity while $\tilde{V}_{\text{anh},3}$ has odd parity. Therefore, the leading correction comes from 2nd-order perturbation so that

$$E' = \frac{1}{2} \sum_k \omega_k + \mathcal{O}(\hbar). \quad (\text{S6})$$

It follows that

$$E = V_0 + \frac{\hbar}{2} \sum_k \omega_k + \mathcal{O}(\hbar^2) = E^{\text{HOA}} + \mathcal{O}(\hbar^2). \quad (\text{S7})$$

Thus, the energy obtained within HOA captures the leading order of \hbar correction to the total energy.

Here as a side remark, because we start with a particular minimizer \mathbf{u} of the total potential to perform our HOA analysis and \mathbf{u} is not invariant to permutations, our harmonic Hamiltonian no longer has permutation symmetry. This induces a symmetry-breaking HOA wave function Ψ_0 . If one starts with a different minimizer \mathbf{u}_p to perform HOA analysis, one should end up with a different HOA wave function Ψ_p . They are related by a simple permutation, i.e., $\Psi_p(\mathbf{r}_1, \mathbf{r}_2, \dots, \mathbf{r}_N) = \Psi_0(\mathbf{r}_{p_1}, \mathbf{r}_{p_2}, \dots, \mathbf{r}_{p_N})$.

Next, let us consider the spin degrees of freedom and construct the full space-spin wave function. Under HOA, we can construct the antisymmetric full wavefunction through linear combinations of Ψ_p ,

$$\Phi^{\text{HOA}}(\mathbf{r}_1, \mathbf{r}_2, \dots, \mathbf{r}_N; s_1, s_2, \dots, s_N) = \frac{1}{\sqrt{N!}} \sum_p (-1)^{\tau(p)} \Psi_0(\mathbf{r}_{p_1}, \mathbf{r}_{p_2}, \dots, \mathbf{r}_{p_N}) \sigma(s_{p_1}, s_{p_2}, \dots, s_{p_N}). \quad (\text{S8})$$

Here σ is an arbitrary normalized N -electron spin wave function with s_i being the spin of the i th electron; τ is the number of transposition of permutation p . The HOA energy can be computed by taking the following the expectation value,

$$E^{\text{HOA}} = \frac{\langle \Phi^{\text{HOA}} | \hat{H} | \Phi^{\text{HOA}} \rangle}{\langle \Phi^{\text{HOA}} | \Phi^{\text{HOA}} \rangle} = V_0 + \frac{\hbar}{2} \sum_k \omega_k + \mathcal{O}(\hbar^2). \quad (\text{S9})$$

In the derivation of Eq. (S9), we have neglected $\langle \Psi_p | \Psi_{p'} \rangle$ and $\langle \Psi_p | \hat{H} | \Psi_{p'} \rangle$ for $p \neq p'$ since Ψ_0 approaches a product of δ -functions at distinct locations when \hbar is sufficiently small. Eq. (S9) is essentially the same as our spinless HOA result. This means that spin only affects higher-order terms of \hbar in the semiclassical limit, which is reasonable because particles behave

classically and quantum effects such as spin splitting become negligible. This is also the case for nuclei, where different nuclear spin states differ tiny little bit in energy, detectable only by nuclear magnetic resonance (NMR).

II. SUPPLEMENTARY RESULTS OF \hbar_{eff} CALCULATIONS

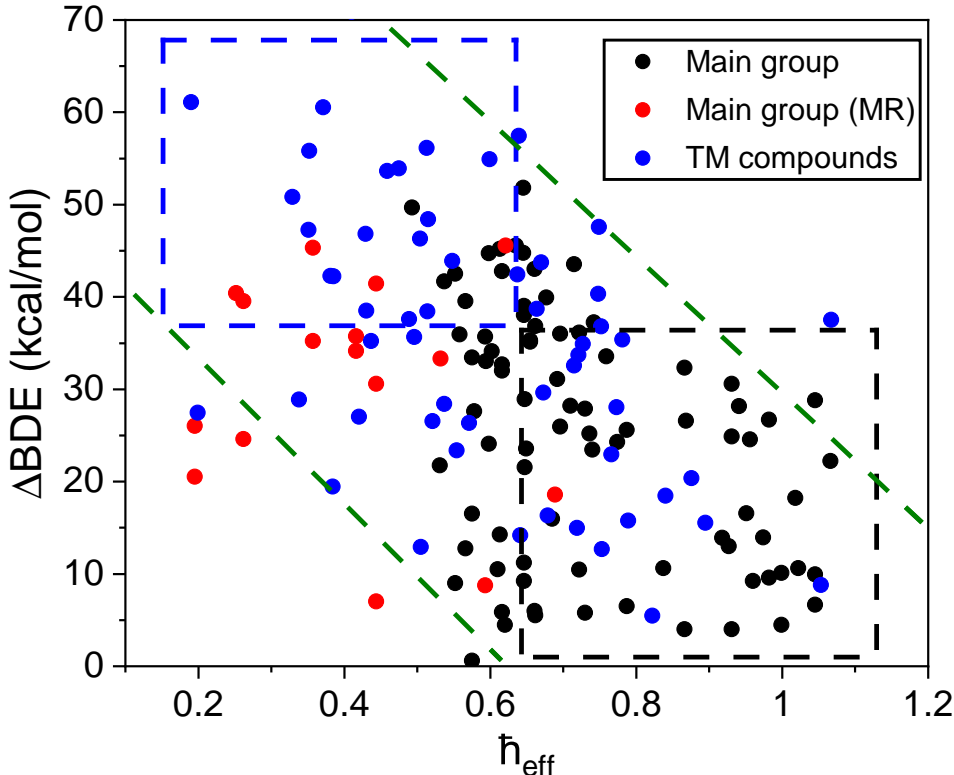


FIG. S1: Scatter plot illustrating the correlated relation between \hbar_{eff} and the error of LDA functional in the prediction of bond dissociation energies (BDEs). Black and red dots: nonmultireference and multireference subsets, respectively, of the BDE99 dataset [1, 2] composed of main group elements. Blue dots: diatomic molecules containing third-row transition-metals (TMs), including TM oxides [3], hydrides [4], nitrides and dimers [5]. The dashed lines and boxes serve as guides of the eye, highlighting the general trend; see the text for details.

In order to evaluate \hbar_{eff} for a molecule, we need to calculate $\tau = \frac{n_L}{n_H}$ from the natural occupation numbers. And these numbers are obtained through complete active space self-consistent field (CASSCF) calculations. Although CASSCF results are known to depend on the choice of active space and basis set, in our practice we find that given a reasonable choice based on our chemical intuition the N th and $(N+1)$ th natural occupation number (n_H and n_L) are not very sensitive to the change of active space or basis set, whereas such changes

do have a great influence on those very small natural occupation numbers. Therefore, we believe CASSCF calculation is sufficient to prove our concept of \hbar_{eff} and correlating it with the errors of bond dissociation energies (BDEs). All of our calculations were performed using PySCF [6–8] with the def2-QZVPPD basis set.[9] Our data set consists of main-group compounds in the BDE99 data set [1, 2] and transition-metal (TM) diatomic molecules including oxides [3], hydrides [4], nitrides and dimers [5]. In total, 145 molecules with 172 types of bond-breaking processes are considered. For some of the molecules such as HOCl, data are available for two types of bond-breaking processes, namely H-OC1 and HO-Cl.

In Fig.S1, we supplement the BDE errors for the local density approximation (LDA) functional, [10] and show its correlation with \hbar_{eff} . The LDA results are similar to PBE shown in the main text; typical weakly and strongly correlated compounds have been enclosed by the black and blue box, respectively. Here the general trend is that data points are dispersed in a band region enclosed by the green reference lines, suggesting a stronger correlation between the LDA error and \hbar_{eff} .

In Table S1, we further supplement the BDE values of PBE, LDA and the reference along with \hbar_{eff} for the molecules tested. For a bond dissociation in A–B, the DFA result is calculated by

$$E_{\text{BDE}}^{\text{DFA}} \equiv E^{\text{DFA}}(\text{A}) + E^{\text{DFA}}(\text{B}) - E^{\text{DFA}}(\text{A-B}). \quad (\text{S10})$$

The reference BDE values are either extracted from high-level calculations [1] or experimental data [3–5], where in the later case all the energy corrections beyond the electronic Schrödinger equation, including the zero-point energies (ZPEs), the relativistic corrections, etc., have been deducted in order to compare the electronic energy.

TABLE S1: Supplementary data of bond dissociation energies (BDEs), signed errors of DFAs (in kcal/mol) and \hbar_{eff} of 145 molecules with 172 types of bond-breaking. For some molecules, our LDA calculations fail to converge. In such cases, we use the literature data when available (in italic) and leave blank otherwise.

Compound	Reference	PBE	PBE error	LDA	LDA error	\hbar_{eff}
Nonmultireference subset of BDE99						
H-OC1	100.8 [1]	94.0	-6.8	<i>106.6</i> [1]	+5.8	0.73
HO-Cl	59.0 [1]	65.5	+6.5	<i>86.9</i> [1]	+27.9	0.73
HO-F	51.5 [1]	62.4	+10.9	87.1	+35.7	0.59
O-NO	75.1 [1]	97.7	+22.6	<i>124.8</i> [1]	+49.7	0.49
N-NO	118.1 [1]	138.6	+20.5	<i>162.9</i> [1]	+44.8	0.65
NN-O	42.4 [1]	67.0	+24.7	94.2	+51.8	0.65
H-ONO	84.8 [1]	75.9	-8.9	85.4	+0.6	0.58

TABLE S1. (*Continued.*)

Compound	Reference	PBE	PBE error	LDA	LDA error	\hbar_{eff}
HO-NO	52.7 [1]	63.7	+11.0	86.1 [1]	+33.4	0.58
H-NC	116.9 [1]	113.9	-3.0	127.3	+10.5	0.72
HN-C	215.1 [1]	222.9	+7.8	251.2	+36.1	0.72
HO-NC	61.6 [1]	69.2	+7.6	92.7	+31.1	0.69
HN-CO	91.9 [1]	107.0	+15.1	131.8	+39.9	0.68
HC-NO	128.0 [1]	144.2	+16.2	172.7 [1]	+44.7	0.60
H-NO	53.1 [1]	51.2	-1.9	62.1 [1]	+9.0	0.55
HN-O	122.8 [1]	134.8	+12.0	165.3	+42.5	0.55
HO-CH ₃	98.4 [1]	100.1	+1.7	123.0	+24.6	0.96
HC-OH	131.1 [1]	137.7	+6.7	163.4	+32.3	0.87
HCO-H	43.1 [1]	37.1	-5.9	47.1	+4.0	0.87
HCO-OH	115.3 [1]	117.1	+1.8	140.5	+25.2	0.74
H ₂ CC-O	173.5 [1]	188.5	+15.0	216.3	+42.8	0.62
H ₂ C-CO	83.0 [1]	94.6	+11.6	115.7	+32.7	0.62
OHC-CHO	76.3 [1]	72.6	-3.6	86.8	+10.5	0.61
H ₃ C-CHO	90.6 [1]	89.2	-1.3	106.5	+16.0	0.69
F ₂ C-O	161.9 [1]	171.1	+9.2	199.1	+37.2	0.74
OHC-F	124.3 [1]	128.4	+4.1	152.5	+28.2	0.71
OHC-H	95.2 [1]	90.7	-4.6	100.8	+5.5	0.66
H ₂ C-O	183.9 [1]	191.3	+7.4	220.7	+36.8	0.66
H-CO	19.7 [1]	26.3	+6.6	34.0	+14.3	0.61
HC-O	195.2 [1]	210.5	+15.3	240.4	+45.2	0.61
SC-S	108.6 [1]	121.6	+13.1	141.6	+33.0	0.59
OC-O	130.4 [1]	147.1	+16.7	174.0	+43.6	0.72
H ₂ C-NH ₂	108.9 [1]	113.1	+4.1	135.6	+26.7	0.98
H ₂ CNH-H	42.8 [1]	44.3	+1.4	52.4	+9.6	0.98
H ₃ C-NH	83.7 [1]	89.0	+5.3	108.6	+24.9	0.93
H-CH ₂ NH	35.2 [1]	35.4	+0.2	39.2	+4.0	0.93
H-CH ₂ NH ₂	100.0 [1]	94.6	-5.4	104.5	+4.5	1.00
CH ₃ NH-H	107.7 [1]	103.4	-4.2	117.8	+10.1	1.00
H-CHNH	103.2 [1]	97.8	-5.3	107.7	+4.5	0.62
HC-NH	168.9 [1]	181.0	+12.1	208.5	+39.5	0.57
HCN-H	22.8 [1]	27.9	+5.1	35.6	+12.7	0.57
H-CN	132.1 [1]	128.8	-3.3	141.3	+9.2	0.65
HC-N	229.2 [1]	241.6	+12.4	268.2	+39.0	0.65
NC-CN	139.3 [1]	143.5	+4.1	161.1	+21.8	0.53
H-SH	96.2 [1]	94.1	-2.1	106.8	+10.6	0.84
HOO-H	93.6 [1]	87.0	-6.5	99.4	+5.9	0.62
HO-OH	54.7 [1]	62.3	+7.6	86.7	+32.0	0.62
S-SH	77.4 [1]	85.5	+8.1	103.0	+25.6	0.79
SS-H	60.9 [1]	58.2	-2.6	67.4	+6.5	0.79
O-OH	68.3 [1]	85.1	+16.8	111.3	+43.0	0.66
OO-H	54.7 [1]	51.4	-3.3	60.7	+6.0	0.66
H-OH	125.8 [1]	124.4	-1.4	142.3	+16.6	0.95
HN-NN	20.2 [1]	41.0	+20.8	65.7	+45.5	0.64
H ₂ N-NH ₂	73.1 [1]	75.7	+2.6	99.7	+26.6	0.87
HN-NH	130.3 [1]	137.7	+7.4	166.3	+35.9	0.56
N-NH	141.8 [1]	158.8	+17.0	183.5	+41.7	0.54
H ₂ N-Cl	65.5 [1]	69.7	+4.3	89.8 [1]	+24.3	0.77

TABLE S1. (*Continued.*)

Compound	Reference	PBE	PBE error	LDA	LDA error	\hbar_{eff}
H ₂ N-H	115.4 [1]	113.3	-2.1	129.4	+13.9	0.97
HN-H	99.5 [1]	100.2	+0.7	112.5	+13.0	0.93
H ₂ CC-CH ₂	153.4 [1]	159.8	+6.4	181.0	+27.6	0.58
HCC-CH ₃	131.6 [1]	133.9	+2.3	153.1	+21.6	0.65
H ₂ CCH-CH ₃	107.6 [1]	105.7	-1.9	124.2	+16.5	0.58
H ₂ CCH-F	127.8 [1]	131.9	+4.1	156.6	+28.8	1.05
H ₃ C-CH ₃	97.3 [1]	96.8	-0.6	115.6	+18.2	1.02
H ₂ C-CH ₂	182.6 [1]	182.5	-0.1	206.7	+24.1	0.60
H ₂ CC-H	86.2 [1]	88.4	+2.2	96.1	+9.9	1.05
H-HCCH	40.6 [1]	43.0	+2.5	47.2	+6.6	1.05
H ₂ C-C	169.2 [1]	175.0	+5.8	198.1	+28.9	0.65
HCC-F	132.3 [1]	141.2	+8.9	167.6	+35.3	0.66
HC-CF	181.5 [1]	188.6	+7.0	216.7	+35.1	0.66
HCC-H	139.4 [1]	137.8	-1.5	150.6	+11.2	0.65
HC-CH	237.1 [1]	245.5	+8.4	275.1	+38.0	0.65
H ₃ C-F	115.1 [1]	119.1	+4.0	143.3	+28.2	0.94
H ₃ C-H	112.6 [1]	110.0	-2.5	123.2	+10.6	1.02
H ₂ C-H	117.1 [1]	115.4	-1.7	126.4	+9.2	0.96
HC-H	106.5 [1]	109.8	+3.3	120.4	+13.9	0.92
FC-F	126.1 [1]	131.3	+5.2	156.7	+30.6	0.93
Cl-CN	104.1 [1]	109.2	+5.1	127.7 [1]	+23.6	0.65
H ₃ B-BH ₃	44.5 [1]	51.4	+7.0	66.7	+22.2	1.07
SS-O	104.5 [1]	113.3	+8.7	140.5	+36.0	0.70
S-SO	82.3 [1]	87.4	+5.1	108.3	+26.0	0.70
O ₂ S-O	86.3 [1]	94.4	+8.0	119.9	+33.6	0.76
OS-O	134.2 [1]	139.2	+5.1	168.3	+34.1	0.60
PP-PP	55.4 [1]	65.7	+10.4	78.8	+23.5	0.74
Multireference subset of BDE99						
F-OOF	17.7 [1]	31.1	+13.5	51.8	+34.2	0.42
FO-OF	46.2 [1]	62.3	+16.0	82.0	+35.7	0.42
O-ClO	62.7 [1]	80.0	+17.3	108.2 [1]	+45.6	0.62
ClO-O	60.9 [1]	79.8	+18.9	100.5 [1]	+39.5	0.26
Cl-OO	5.6 [1]	17.6	+12.1	30.2 [1]	+24.6	0.26
FO-O	81.7 [1]	103.0	+21.3	127.0	+45.3	0.36
F-OO	13.9 [1]	31.2	+17.3	49.1	+35.2	0.36
ClO-Cl	36.0 [1]	38.0	+2.0	54.6 [1]	+18.6	0.69
FO-F	40.7 [1]	51.5	+10.8	74.0	+33.3	0.53
H-OF	105.6 [1]	100.4	-5.2	114.4	+8.8	0.59
HOO-O	57.8 [1]	76.8	+19.0	99.2	+41.5	0.44
HO-OO	5.3 [1]	18.3	+13.0	35.8	+30.6	0.44
H-OOO	85.9 [1]	86.9	+1.1	92.9	+7.0	0.44
OO-O	26.6 [1]	41.3	+14.7	67.0	+40.4	0.25
SSS-S	66.0 [1]	74.0	+8.0	92.0	+26.0	0.20
SS-SS	25.9 [1]	28.8	+3.0	46.4	+20.5	0.20
Transition-metal compounds						
ScO	161.9 [3]	184.4	+22.6	209.4	+47.6	0.75
TiO	160.4 [3]	188.1	+27.7	215.3	+54.9	0.60
VO	153.5 [3]	183.1	+29.6			0.51
CrO	106.7 [3]	120.8	+14.0			0.45

TABLE S1. (*Continued.*)

Compound	Reference	PBE	PBE error	LDA	LDA error	\hbar_{eff}
MnO	88.4 [3]	126.5	+38.1	148.9	+60.5	0.37
FeO	99.7 [3]	128.5	+28.8			0.34
CoO	91.6 [3]	115.1	+23.4			0.35
NiO	86.1 [3]	112.8	+26.7			0.35
CuO	66.6 [3]	77.9	+11.3	95.5	+28.9	0.34
ZnO	39.8 [3]	46.9	+7.2	66.3	+26.5	0.52
YO	171.1 [3]	181.7	+10.6	206.5	+35.4	0.78
ZrO	184.1 [3]	198.9	+14.8	224.4	+40.3	0.75
NbO	174.8 [3]	192.1	+17.2			0.70
MoO	126.7 [3]	141.0	+14.2			0.51
TcO	131.2 [3]	146.0	+14.8	169.6	+38.4	0.51
RuO	127.0 [3]	134.8	+7.7	162.7	+35.7	0.50
RhO	98.3 [3]	121.1	+22.8	151.9	+53.6	0.46
PdO	55.7 [3]	81.3	+25.6	102.6	+46.8	0.43
AgO	52.8 [3]	55.9	+3.1	71.3	+18.5	0.84
CdO	23.1 [3]	29.0	+5.9	38.9	+15.8	0.79
HfO	196.4 [3]	205.7	+9.3	235.2	+38.7	0.66
TaO	202.4 [3]	200.0	-2.4	228.7	+26.4	0.57
WO	169.0 [3]	185.4	+16.4	217.4	+48.4	0.52
OsO	133.1 [3]	138.8	+5.7			0.48
IrO	106.3 [3]	130.3	+24.0			0.51
PtO	94.6 [3]	116.6	+22.0			0.51
AuO	51.5 [3]	63.9	+12.4	84.0	+32.5	0.72
ScO ⁺	165.4 [3]	180.2	+14.7	209.1	+43.7	0.67
TiO ⁺	158.3 [3]	172.6	+14.3	200.8	+42.4	0.64
VO ⁺	136.9 [3]	156.3	+19.4			0.50
CrO ⁺	82.4 [3]	99.1	+16.7	124.6	+42.2	0.39
MnO ⁺	72.6 [3]	83.9	+11.3			0.27
FeO ⁺	83.0 [3]	111.3	+28.3			0.39
CoO ⁺	70.6 [3]	95.9	+25.3	121.4	+50.8	0.33
NiO ⁺	42.3 [3]	84.5	+42.2			0.38
CuO ⁺	26.4 [3]	48.9	+22.5	63.9	+37.5	1.07
ZnO ⁺	39.2 [3]	48.5	+9.3	62.1	+22.9	0.77
YO ⁺	172.1 [3]	189.3	+17.2	208.9	+36.8	0.75
ZrO ⁺	180.7 [3]	189.1	+8.3	215.6	+34.9	0.73
NbO ⁺	165.1 [3]	185.6	+20.5			0.67
MoO ⁺	117.1 [3]	143.1	+26.1	173.2	+56.1	0.51
RuO ⁺	89.2 [3]	111.0	+21.8	127.7	+38.5	0.43
RhO ⁺	72.9 [3]	96.7	+23.9			0.41
PdO ⁺	35.2 [3]	74.4	+39.2			0.44
AgO ⁺	29.0 [3]	24.1	-4.9	37.8	+8.8	1.05
HfO ⁺	180.2 [3]	185.1	+5.0	213.9	+33.7	0.72
TaO ⁺	188.7 [3]	188.4	-0.3	218.3	+29.6	0.67
WO ⁺	169.8 [3]	183.8	+14.0			0.62
ReO ⁺	100.3 [3]	120.3	+20.0			0.52
OsO ⁺	95.6 [3]	125.7	+30.1			0.33
IrO ⁺	104.8 [3]	122.9	+18.1	151.1	+46.3	0.50
PtO ⁺	78.8 [3]	104.0	+25.3	132.7	+53.9	0.48
AuO ⁺	18.6 [3]	54.0	+35.4	76.0	+57.5	0.64

TABLE S1. (*Continued.*)

Compound	Reference	PBE	PBE error	LDA	LDA error	\hbar_{eff}
ScH	51.4 [4]	54.4	+3.1	64.3	+12.9	0.51
TiH	53.6 [4]	65.6	+12.1	73.9	+20.4	0.88
VH	54.6 [4]	74.1	+19.5	82.7 [4]	+28.1	0.77
CrH	46.2 [4]	52.5	+6.3	60.4	+14.2	0.64
MnH	34.2 [4]	45.3	+11.1	49.8	+15.5	0.90
FeH	43.2 [4]	56.2	+12.9	66.6 [4]	+23.4	0.55
CoH	53.4 [4]	60.7	+7.4	72.8	+19.5	0.38
NiH	62.1 [4]	66.7	+4.6	78.4 [4]	+16.3	0.68
CuH	60.6 [4]	64.6	+4.0	75.6	+15.0	0.72
ZnH	23.9 [4]	23.0	-0.9	29.3	+5.5	0.82
Ti ₂	37.3 [5]	77.2	+39.9	108.2	+70.9	0.41
V ₂ ⁺	73.2 [5]	105.9	+32.7	129.0 [5]	+55.8	0.35
V ₂	65.8 [5]	105.4	+39.6	113.1 [5]	+47.3	0.35
Cr ₂	35.3 [5]	24.6	-10.7	62.7	+27.4	0.20
Fe ₂	27.8 [5]	57.3	+29.6	88.8 [5]	+61.1	0.19
Cu ₂	47.5 [5]	49.0	+1.5	60.1	+12.7	0.75
ScN	115.3 [5]	123.8	+8.5	143.7	+28.4	0.54
TiN	127.0 [5]	144.6	+17.7	170.8	+43.9	0.55
VN	120.0 [5]	147.1	+27.2	157.5 [5]	+37.6	0.49
CrN	100.0 [5]	106.3	+6.3	127.0	+27.0	0.42

III. SOME DETAILS OF DFA CALCULATIONS IN THE SEMICLASSICAL LIMIT

By the energy scaling argument in the main text, the energy functional (E_{\hbar}) for $\hbar \neq 1$ and for $\hbar = 1$ (E_1) are related by the following equation,

$$E_{\hbar}[\rho_{\hbar}] = \frac{1}{\hbar^2} E_1[\rho_1]. \quad (\text{S11})$$

Here ρ_{\hbar} is an arbitrary v -representable density for the problem $\hbar \neq 1$, and $\rho_1(\mathbf{r}) = \hbar^6 \rho_{\hbar}(\hbar^2 \mathbf{r})$ is the scaled density. Eq. (S11) can be viewed as the defining equation for E_{\hbar} .

By the Kohn-Sham decomposition,

$$E_1[\rho_1] = T_{s,1}[\rho_1] + V_{\text{ext},1}[\rho_1] + J_1[\rho_1] + E_{xc,1}[\rho_1]. \quad (\text{S12})$$

Let us analyze terms on the RHS one by one.

$$V_{\text{ext},1}[\rho_1] = \int \hbar^6 \rho_{\hbar}(\hbar^2 \mathbf{r}) V_{\text{ext},1}(\mathbf{r}) d\mathbf{r} = \hbar^2 \int \rho_{\hbar}(\mathbf{r}') V_{\text{ext},\hbar}(\mathbf{r}') d\mathbf{r}'. \quad (\text{S13})$$

Here we have used $V_{\text{ext},1}(\mathbf{r}) = \hbar^2 V_{\text{ext},\hbar}(\hbar^2 \mathbf{r})$ and change of variable $\mathbf{r}' = \hbar^2 \mathbf{r}$. By the same

argument,

$$J_1[\rho_1] = \frac{1}{2} \int \frac{\rho_1(\mathbf{r})\rho_1(\mathbf{r}')}{|\mathbf{r} - \mathbf{r}'|} d\mathbf{r}d\mathbf{r}' = \frac{1}{2} \int \frac{\hbar^6 \rho_h(\hbar^2 \mathbf{r}) \hbar^6 \rho_h(\hbar^2 \mathbf{r}')}{|\mathbf{r} - \mathbf{r}'|} d\mathbf{r}d\mathbf{r}' = \frac{1}{2} \hbar^2 \int \frac{\rho_h(\mathbf{r})\rho_h(\mathbf{r}')}{|\mathbf{r} - \mathbf{r}'|} d\mathbf{r}d\mathbf{r}'. \quad (\text{S14})$$

The Kohn-Sham kinetic energy calculation is slightly more complicated because it involves the Kohn-Sham orbitals. However, because the problem of $\hbar \neq 1$ and $\hbar = 1$ are equivalent up to a scaling of coordinate, the corresponding Kohn-Sham orbitals shall also have similar relations, i.e., $\phi_{i,1}(\mathbf{r}) = \hbar^3 \phi_{i,h}(\hbar^2 \mathbf{r})$. It follows that

$$\begin{aligned} T_{s,1}[\rho_1] &= -\frac{1}{2} \sum_i^{\text{occ.}} \int \phi_{i,1}^*(\mathbf{r}) \nabla^2 \phi_{i,1}(\mathbf{r}) d\mathbf{r} = -\frac{\hbar^6}{2} \sum_i^{\text{occ.}} \int \phi_{i,h}^*(\hbar^2 \mathbf{r}) \nabla^2 \phi_{i,h}(\hbar^2 \mathbf{r}) d\mathbf{r} \\ &= -\frac{\hbar^2}{2} \sum_i^{\text{occ.}} \int \phi_{i,h}^*(\mathbf{r}) \nabla^2 \phi_{i,h}(\mathbf{r}) d\mathbf{r}. \end{aligned} \quad (\text{S15})$$

Substituting Eqs. (S13)–(S15) into Eq. (S12) and comparing with Eq. (S11), we have

$$\begin{aligned} E_h[\rho_h] &= -\frac{1}{2} \sum_i^{\text{occ.}} \int \phi_{i,h}^*(\mathbf{r}) \nabla^2 \phi_{i,h}(\mathbf{r}) d\mathbf{r} + \int \rho_h(\mathbf{r}') V_{\text{ext},1}(\mathbf{r}') d\mathbf{r}' + \frac{1}{2} \int \frac{\rho_h(\mathbf{r})\rho_h(\mathbf{r}')}{|\mathbf{r} - \mathbf{r}'|} d\mathbf{r}d\mathbf{r}' + \frac{1}{\hbar^2} E_{xc,1}[\rho_1] \\ &= T_{s,1}[\rho_h] + V_{\text{ext},1}[\rho_h] + J_1[\rho_h] + \frac{1}{\hbar^2} E_{xc,1}[\rho_1]. \end{aligned} \quad (\text{S16})$$

This suggests that in the evaluation of E_h for a given density, we only have to plug the density directly into the functional form of E_1 except the xc functional, which should be replaced by

$$E_{xc,h}[\rho_h] = \frac{1}{\hbar^2} E_{xc,1}[\rho_1]. \quad (\text{S17})$$

Eq. (S17) shall be viewed as the defining equation for the xc functional for $\hbar \neq 1$. This is true for the exact xc functional as well as DFAs. In addition, for most of the mainstream DFA exchange as well as the exact exchange functional, one can show that $\frac{1}{\hbar^2} E_{x,1}[\rho_1] = E_{x,1}[\rho_h]$ using our scaling arguments above or the uniform scaling equality [11]. This further reduces the re-scaling definition to only the correlation functional,

$$E_{xc,h}[\rho_h] = E_{x,1}[\rho_h] + \frac{1}{\hbar^2} E_{c,1}[\rho_1], \quad (\text{S18})$$

As a side remark, Eq. (S17) can also be derived from the constrained search definition of the exact functional [12], which is in similar spirit to the derivation of the scaling relation with respect to the interaction strength λ [13].

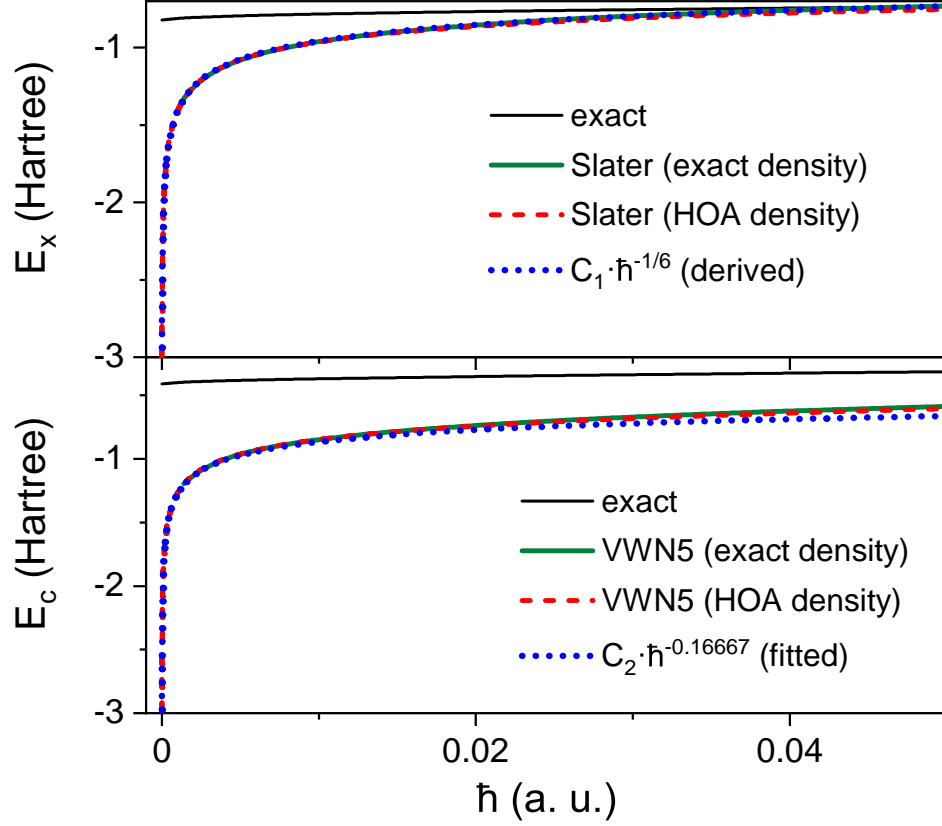


FIG. S2: LDA exchange (Slater) and correlation (VWN5) energy for harmonium as $\hbar \rightarrow 0$, in comparison with the exact results. The blue dotted curves show the asymptotic behavior of LDA.

IV. SOME DETAILS OF THE ASYMPTOTIC LEADING TERM OF LDA

Here we give a brief derivation of the asymptotic $\mathcal{O}(\hbar^{-1/6})$ behavior of the LDA exchange energy in the limit $\hbar \rightarrow 0$ for model atoms. Taking harmonium with $\lambda = 1$ and arbitrary ω for an example, the ground state density under HOA can be written as

$$\rho_{\text{HOA}} = \frac{B}{\sqrt{\hbar}} \exp \left[-\frac{a}{\hbar} (r - r_0)^2 \right]. \quad (\text{S19})$$

Here $B = 2 \times \frac{1}{4\pi r_0^2} \sqrt{\frac{a}{\pi}}$, $a = (3 - \sqrt{3})\omega$ and $r_0 = (2\omega)^{-2/3}$. As the main text shows, ρ_{HOA} is an extremely good approximation to the exact density in approaching the semiclassical limit. Substituting ρ_{HOA} into the LDA (Slater) exchange functional, we can obtain that

$$E_x^{\text{LDA}}[\rho_{\text{HOA}}] = -C_x \int \rho_{\text{HOA}}^{\frac{4}{3}} d\mathbf{r} = -\frac{4\pi C_x B^{\frac{4}{3}}}{\hbar^{2/3}} \int_0^\infty \exp \left[-\frac{4a}{3\hbar} (r - r_0)^2 \right] r^2 dr. \quad (\text{S20})$$

As $\hbar \rightarrow 0$, the integrand contains an extremely narrow Gaussian centered in the positive r region, which can be well approximated by

$$\int_0^\infty \exp \left[-\frac{4a}{3\hbar}(r - r_0)^2 \right] r^2 dr \approx \int_{-\infty}^\infty \exp \left[-\frac{4a}{3\hbar}(r - r_0)^2 \right] r_0^2 dr = r_0^2 \sqrt{\frac{3\pi\hbar}{4a}}. \quad (\text{S21})$$

Therefore,

$$E_x^{\text{LDA}}[\rho_{\text{HOA}}] \approx -\mathcal{O}\left(\hbar^{-\frac{1}{6}}\right). \quad (\text{S22})$$

The VWN5 correlation has more complicated functional form, which is difficult to analytically determine the leading-order divergence. Nevertheless, by fitting the numerical results with small \hbar 's, we find that it has similar $\mathcal{O}(\hbar^{-1/6})$ behavior.

The above conclusions have been verified in Fig.S2. Substituting the exact or HOA density into the LDA exchange (and also correlation) functional essentially leads to the same result for small \hbar , and they all agree with the $\mathcal{O}(\hbar^{-1/6})$ asymptotic behavior, strongly deviating from the exact curves. Here for 2-electron spin-unpolarized problem, the exact exchange has simple relation with the Hartree energy as $E_x^{\text{exact}} = -\frac{1}{2}J$. The exact correlation energy can be then calculated by $E_c^{\text{exact}} = E_{xc}^{\text{exact}} - E_x^{\text{exact}}$.

For 2-electron diatomic molecular models, similarly, the ground state density can be approximated by the following HOA expression written in cylindrical coordinates,

$$\rho_{\text{mol}} \approx \frac{A}{\hbar} \exp \left[-\frac{b}{\hbar} z^2 - \frac{c}{\hbar} (s - s_0)^2 \right]. \quad (\text{S23})$$

Here s and z are the radial distance and axial coordinate, respectively; $A = 2 \times \frac{1}{2\pi s_0^2} \sqrt{\frac{bc}{\pi^2}}$, b, c and s_0 are constants that depend on the model potential. In analogy to Eq. (S22),

$$E_x^{\text{LDA}}[\rho_{\text{mol}}] = -C_x \int \rho_{\text{mol}}^{4/3} d\mathbf{r} \approx -\frac{2\pi C_x A^{4/3}}{\hbar^{4/3}} \int_{-\infty}^\infty dz \int_0^\infty s ds \exp \left[-\frac{4b}{3\hbar} z^2 - \frac{4c}{3\hbar} (s - s_0)^2 \right]. \quad (\text{S24})$$

Here

$$\begin{aligned} \int_{-\infty}^\infty dz \exp \left[-\frac{4b}{3\hbar} z^2 \right] &= \sqrt{\frac{3\pi\hbar}{4b}}, \\ \int_0^\infty s ds \exp \left[-\frac{4c}{3\hbar} (s - s_0)^2 \right] &\approx s_0 \sqrt{\frac{3\pi\hbar}{4c}}. \end{aligned} \quad (\text{S25})$$

Therefore,

$$E_x^{\text{LDA}}[\rho_{\text{mol}}] \approx -\mathcal{O}\left(\hbar^{-\frac{1}{3}}\right). \quad (\text{S26})$$

For the correlation energy, one can numerically verify that the asymptotic leading term is also $\mathcal{O}(\hbar^{-1/3})$ by substituting Eq. (S23) into the VWN5 functional.

Moreover, we can show that the Hartree term for diatomic molecules also diverges in the semiclassical limit. We prove this by calculating the integral in the \mathbf{k} space. The Fourier transform of ρ_{mol} can be calculated using the similar technique of Eq. (S24)–(S25), giving

$$\tilde{\rho}(\mathbf{k}) = \frac{1}{(2\pi)^{3/2}} \int \rho_{\text{mol}}(\mathbf{r}) e^{i\mathbf{k}\cdot\mathbf{r}} d\mathbf{r} \approx \frac{2}{(2\pi)^{3/2}} J_0(s_0 k_s) \exp\left(-\frac{\hbar}{4b} k_z^2\right), \quad (\text{S27})$$

where k_s and k_z are the radial distance and axial coordinate in the reciprocal space, J_0 is the Bessel function of the first kind. The Hartree term is given by

$$J = \frac{1}{2} \int \frac{4\pi}{k^2} |\tilde{\rho}(\mathbf{k})|^2 d\mathbf{k} \approx \frac{4}{\pi} \int_0^{+\infty} dk_z \cdot \exp\left(-\frac{\hbar}{2b} k_z^2\right) \int_0^\infty k_s dk_s \cdot [J_0(s_0 k_s)]^2 \frac{1}{k_s^2 + k_z^2}. \quad (\text{S28})$$

Here we have used the fact that the integrand is an even function of k_z . Moreover, one can show that integration over the large- k_z region makes J blow up when $\hbar \rightarrow 0$. To analyze the leading order divergence, it suffices to replace the lower limit of 0 by 1 (to avoid singularity in the subsequent steps) in the integration over k_z and analyze the asymptotic behavior of the second integral in Eq. (S28) as a function of k_z . In particular, one can show that

$$\int_0^\infty dk_s \cdot k_s [J_0(s_0 k_s)]^2 \frac{1}{k_s^2 + k_z^2} \approx \frac{1}{2k_z s_0}. \quad (\text{S29})$$

In deriving Eq. (S29), we have used $k_s [J_0(s_0 k_s)]^2 \approx \frac{1}{\pi s_0} [1 + \sin(2s_0 k_s)]$. Here $\sin(2s_0 k_s)$ is an oscillatory function of k_s , giving negligible contribution to the integral when multiplied by $\frac{1}{k_s^2 + k_z^2}$; replacing $k_s [J_0(s_0 k_s)]^2$ by $k_s [J_0(s_0 k_s)]^2$ yields the final result of $\frac{1}{2k_z s_0}$. Using the above arguments in Eq. (S28), we have

$$J \approx \frac{4}{\pi} \int_1^{+\infty} dk_z \cdot \exp\left(-\frac{\hbar}{2b} k_z^2\right) \frac{1}{2k_z s_0}. \quad (\text{S30})$$

The approximate formula for J is \hbar -dependent. To better understand its \hbar -dependence, particularly for small \hbar , we evaluate

$$\frac{dJ}{d\hbar} = -\frac{4}{\pi} \int_1^{+\infty} dk_z \cdot \exp\left(-\frac{\hbar}{2b} k_z^2\right) \frac{k_z}{4bs_0} = -\frac{1}{\pi s_0} \frac{1}{\hbar} e^{-\frac{\hbar}{2b}} = -\frac{1}{\pi s_0} \frac{1}{\hbar} + \mathcal{O}(1). \quad (\text{S31})$$

This suggests that

$$J = \frac{1}{\pi s_0} |\ln \hbar| + \mathcal{O}(1), \quad (\text{S32})$$

which has been verified by numerical results.

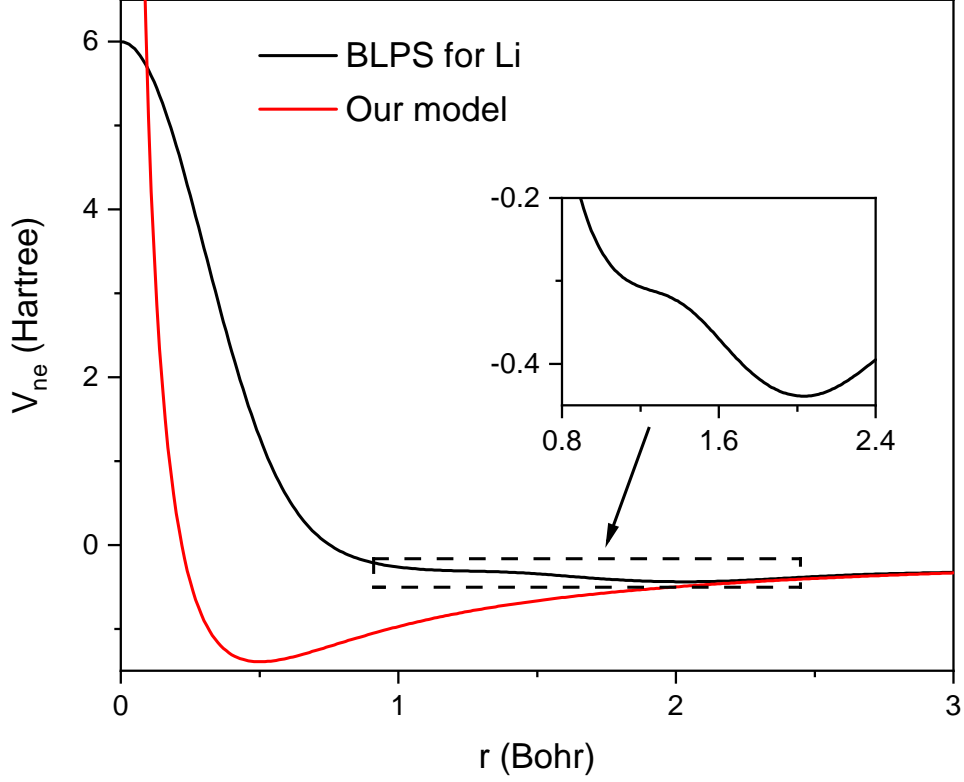


FIG. S3: Our self-designed effective potential as a function of electron-nuclear distance in comparison with the BLPS potential for lithium. The inset shows an enlarged plot of the intermediate region of BLPS to better visualize the fine details.

V. SUPPLEMENTARY FIGURE SHOWING OUR EFFECTIVE POTENTIAL FOR DIATOMIC MOLECULAR MODEL

In Fig. S3, we compare our self-designed effective electron-nuclear potential for simulating single-bond stretching of a diatomic molecule with the bulk-derived local pseudopotential (BLPS) [14] for Li atom. Our potential has the following analytic form,

$$V_{\text{reff}}(r) = -\frac{e^{\beta r} - 1}{e^{\beta r} + 1} \frac{1}{r} + \frac{2}{e^{\beta r} + 1} \frac{1}{r}, \quad (\text{S33})$$

where $\beta = 5$ is an adjustable parameter. Such a form bridges the short-range repulsion and long-range attraction of the BLPS through a simple Fermi-Dirac function, and smooths out the fine details in the intermediate region in order to simplify the physical picture. This suffices for our need of proving concept.

References

- [1] Mardirossian, N.; Head-Gordon, M. Thirty years of density functional theory in computational chemistry: an overview and extensive assessment of 200 density functionals. *Mol. Phys.* **2017**, *115*, 2315–2372.
- [2] Karton, A.; Daon, S.; Martin, J. M. L. W4-11: A high-confidence benchmark dataset for computational thermochemistry derived from first-principles W4 data. *Chem. Phys. Lett.* **2011**, *510*, 165–178.
- [3] Moltved, K. A.; Kepp, K. P. The Chemical Bond between Transition Metals and Oxygen: Electronegativity, d-Orbital Effects, and Oxophilicity as Descriptors of Metal–Oxygen Interactions. *J. Phys. Chem. C* **2019**, *123*, 18432–18444.
- [4] Moltved, K. A.; Kepp, K. P. Chemical Bond Energies of 3d Transition Metals Studied by Density Functional Theory. *J. Chem. Theory Comput.* **2018**, *14*, 3479–3492.
- [5] Furche, F.; Perdew, J. P. The performance of semilocal and hybrid density functionals in 3d transition-metal chemistry. *J. Chem. Phys.* **2006**, *124*.
- [6] Sun, Q. Libcint: An efficient general integral library for Gaussian basis functions. *J. Comput. Chem.* **2015**, *36*, 1664–1671.
- [7] Sun, Q.; Berkelbach, T. C.; Blunt, N. S.; Booth, G. H.; Guo, S.; Li, Z.; Liu, J.; McClain, J. D.; Sayfutyarova, E. R.; Sharma, S.; Wouters, S.; Chan, G. K.-L. PySCF: the Python-based simulations of chemistry framework. *Wiley Interdiscip. Rev. Comput. Mol. Sci.* **2018**, *8*, e1340.
- [8] Sun, Q. et al. Recent developments in the PySCF program package. *J. Chem. Phys.* **2020**, *153*, 024109.
- [9] Weigend, F.; Furche, F.; Ahlrichs, R. Gaussian basis sets of quadruple zeta valence quality for atoms H–Kr. *J. Chem. Phys.* **2003**, *119*, 12753–12762.
- [10] Vosko, S. H.; Wilk, L.; Nusair, M. Accurate spin-dependent electron liquid correlation energies for local spin density calculations: a critical analysis. *Can. J. Phys.* **1980**, *58*, 1200–1211.
- [11] Levy, M.; Perdew, J. P. Hellmann-Feynman, virial, and scaling requisites for the exact universal density functionals. Shape of the correlation potential and diamagnetic susceptibility for atoms. *Phys. Rev. A* **1985**, *32*, 2010–2021.
- [12] Levy, M. Universal variational functionals of electron densities, first-order density matrices, and natural spin-orbitals and solution of the v-representability problem. *Proc. Natl. Acad. Sci. U.S.A.* **1979**, *76*, 6062–6065.
- [13] Parr, R.; Yang, W. *Density-Functional Theory of Atoms and Molecules*; Oxford University Press, 1994.
- [14] Huang, C.; Carter, E. A. Transferable local pseudopotentials for magnesium, aluminum and silicon. *Phys. Chem. Chem. Phys.* **2008**, *10*, 7109–7120.